J. Fluid Mech. (1996), *vol.* 316, *pp.* 73–113

Disturbance growth in an unstable three-dimensional boundary layer and its dependence on environmental conditions

By H. DEYHLE† AND H. BIPPES

Deutsche Forschungsanstalt für Luft- und Raumfahrt, Institut für Strömungsmechanik, Bunsenstr. 10, D-37073 Göttingen, Germany

(Received 19 April 1995 and in revised form 28 December 1995)

Experimental investigations in the three-dimensional boundary layer of a swept flat plate with the pressure gradient induced from outside are aimed at enhancing knowledge of the transition process in the presence of pure crossflow instability. The development of disturbances is characterized by the occurrence of both stationary and travelling instability modes, by early nonlinear development and by complex dependence upon the environmental conditions. Experiments under natural conditions of transition showed a good correspondence of the identified modes with those predicted by local linear stability theory. The disturbance growth, however, is generally overpredicted. Controlled excitation of crossflow vortices allowing measurements closer to the linear range of amplification confirmed this result. Nonlinear effects such as interaction between stationary disturbances and base flow and between travelling and stationary modes have already been observed when the naturally excited instabilities become of measurable size.

The most striking feature of the disturbance development is the complex dependence on initial conditions. Experiments under systematically varied environments showed that surface roughness represents the key parameter responsible for the initiation of stationary crossflow vortices. In contrast to two-dimensional boundary layers, free-stream turbulence influences the transition process indirectly. Only for turbulence levels $Tu > 0.2\%$ and smooth surfaces do the travelling instability waves dominate. The location of the final breakdown of laminar flow is clearly determined by the saturation amplitude of crossflow vortices. The receptivity to sound, two-dimensional surface roughness and non-uniformities of the test-section mean flow was found to be very weak.

1. Introduction

In accelerated three-dimensional boundary layers crossflow leads to dynamic instability. Oblique travelling waves and stationary vortices are amplified as primary instabilities. Therefore, a complex disturbance motion develops from the beginning of the transition process. According to local linear stability theory the unsteady modes are more amplified than the steady modes. However, in the overwhelmingly majority of crossflow experiments the stationary vortices appeared to be more amplified than the travelling modes (see the review by Reed and Saric 1989). Thus, the three-dimensional boundary-layer flow belongs to the class of flows primarily unstable to streamwise

† Present address: Deutsche Forschungsanstalt für Luft- und Raumfahrt, Institut für Aeroelastik, Bunsenstr. 10, D-37073 Göttingen, Germany.

vortices. Owing to the mean flow distortion by the streamwise vortices, the stability features of the local boundary-layer profiles are changed considerably and the flow becomes susceptible to complicated secondary instability mechanisms.

Comparisons between linear theory and experiment (reviewed by Reed & Saric 1989) have shown that the wavelengths and frequencies of the most unstable instability modes are well predicted. Measurements by Deyhle, Höhler & Bippes (1993) indicate further agreement for the direction of wave propagation. Moreover, Gaponenko, Ivanov & Kachanov (1994) demonstrated in their swept flat plate experiment that for a wave packet generated by a localized impulse the dispersion characteristics of the travelling modes compare well with local linear stability theory. However, a difference in the measured growth of the disturbances has been observed: whereas Kachanov & Tararykin (1990) found good agreement between the amplification rates of the stationary modes measured under controlled conditions and those obtained in a local linear stability analysis, Bippes, Müller & Wagner (1991) as well as Radeztsky, Reibert & Saric (1994) found significant disagreement which is suggested to be due to early nonlinear development. They came to the conclusion that local linear theory is not adequate to describe the transition process in the presence of crossflow instability.

Different observations are also made in the later stages of the transition process. Prior to the onset of transition, on a swept wing in a 0.15% turbulence environment Arnal, Coustols & Juillen (1984) traced stationary vortices with an intensity of 15% of the local inviscid flow and unsteady modes at frequencies up to 200 Hz of 15–20% intensity. Poll (1985) monitored velocity fluctuations having a fundamental frequency of the order of 1 kHz with occasionally appearing oscillations at frequencies one order of magnitude larger than the fundamental frequency. On a swept wing in low-turbulence flow (0.1% turbulence level) Saric and co-workers (summarized in Saric 1994) established the transition process governed by streamwise vortices which cause secondary high-frequency disturbances in the kHz range. An exceptional result was obtained by Takagi & Itoh (1994). On a swept cylinder with a very smooth surface they observed only travelling crossflow modes in two wind tunnels with turbulence levels of 0.15% and 0.046%, respectively.

In view of all these diverse observations the question arises of what determines the disturbance development and transition in flows subject to crossflow instability. This question has motivated the current work, and has guided the design of the experimental set-up. The experiments referred to above, and the experience with other types of flows primarily unstable to streamwise vortices such as Görtler flow, Dean flow, flows in rotating systems and along heated surfaces suggest that the flow development depends on the upstream conditions in combination with the early nonlinear development. Consequently the present investigation was focused on the effect of vortical and sound disturbances of the oncoming wind-tunnel flow and of roughness of the model surface on the development of instabilities. The results can help to clarify the role of the environment and of early nonlinear interaction on the transition process.

In this regard the present work continues the experiments described in the thesis by Müller (1990), details of which are also published in Müller & Bippes (1988), Müller (1989) and Bippes *et al.* (1991), on the same model. His observations, supporting the described hypothesis and inspiring the present work, are discussed in §2. The experimental set-up and the measurement techniques adopted for the present experiments are described in §3. This section also contains the base flow data (§3.1). Section 4 comprises the results and discussion. The most amplified instabilities identified in the experiment are described and compared in §4.1 with those predicted by linear stability theory. The growth of the disturbances, presented in §4.2, is discussed with special

regard to nonlinear aspects in §4.3. Section 4.4 deals with the influence of the various environmental conditions under consideration: free-stream turbulence (§4.4.1), sound (§4.4.2), spatial non-uniformities of the oncoming mean flow (§4.4.3) and surface roughness (§4.4.4). The effect of the relevant environmental disturbances on the final breakdown of laminar flow is shown in §4.5. Concluding remarks are given in §5.

2. Discussion of previous results motivating the present work

Previous experiments and numerical simulations support the hypothesis that environmental conditions and early nonlinear interaction play a key role. Müller (1990) performed extensive flow field measurements on a swept flat plate to trace the downstream development of the disturbance motion under natural conditions of transition. For a free-stream turbulence level of $Tu = 1/Q_\infty[\frac{1}{3}(\overline{u'^2}+\overline{v'^2}+\overline{w'^2})]^{1/2} = 0.15\%$ (measured in the frequency range $2\,\text{Hz} < f < 2\,\text{kHz}$) he found approximately equal growth of stationary $(\bar{u}_s, \bar{v}_s)$ and travelling modes (u_{rms}, v_{rms}) as shown in figure 1(*a*). This result is in contrast to local linear stability theory, which predicts higher amplification rates for travelling modes. However, since growth of both modes is much smaller than predicted by local linear theory and since it attenuates continuously until the disturbance amplitudes end up at a certain saturation level (10% of the inviscid flow for both modes), it is inferred that Müller (1990) observed essentially nonlinear development. The dependence upon the upstream conditions became obvious when the tests were repeated using the identical model in another wind tunnel with a lower free-stream turbulence, $Tu = 0.08\%$ (Müller 1990, see also Müller & Bippes 1988 and Bippes *et al.* 1991). Now, the stationary modes were much more amplified than the travelling modes and the saturation amplitudes became considerably different (figure 1*b*). The stationary modes ended up at amplitudes of 20% whereas the travelling modes only reached 5%. Surprisingly the N-factor (factor of integrated amplification) for transition at the lower turbulence level was found to be only 15, i.e. significantly smaller than the $N = 17$ in the higher turbulence environment.

Another striking feature was the difference in the amplitudes of the travelling modes measured along streamwise zones of $\bar{U}_{s,max}(z) = [\overline{\bar{U}}_s + \bar{u}_s(z)]_{max}$ and $\bar{U}_{s,min}(z) = [\overline{\bar{U}}_s + \bar{u}_s(z)]_{min}$. Here $\bar{U}_s$ is the mean velocity measured in the streamline-orientated coordinate system (figure 4) which comprises the time and spanwise averaged mean flow $\overline{\bar{U}}_s$ and the stationary disturbance $\bar{u}_s$. According to the secondary stability theory by Fischer & Dallmann (1991) this difference is due to the distortion of the mean flow by the streamwise vortices which makes the flow susceptible to secondary instability. Comparison with Müller's experiment revealed that the secondary theory can explain the features observed in the experiment although the tests were performed in a parameter range which is at the limit of the applicability of the theoretical model. It should be noted that the direct numerical simulations of Meyer & Kleiser (1989), Wagner (1992) and Müller, Bestek & Fasel (1994) (for more details see the thesis of W. Müller 1995) not only reproduce the early beginning of nonlinear development but also the strong dependence upon the initial conditions. The nonlinear parabolized stability equations (PSE) analysis by Malik, Li & Chang (1994) for swept wing flow leads to the same conclusions. Thus, the physical features observed in the experiment are well described by nonlinear analyses. However, quantitative comparisons are scarce. They require the precise adjustment of the initial conditions.

All these results indicate that in three-dimensional boundary-layer flows subject to crossflow instability the quantitative description of the transition process up to the breakdown of laminar flow requires the physically relevant initial conditions. Hence,

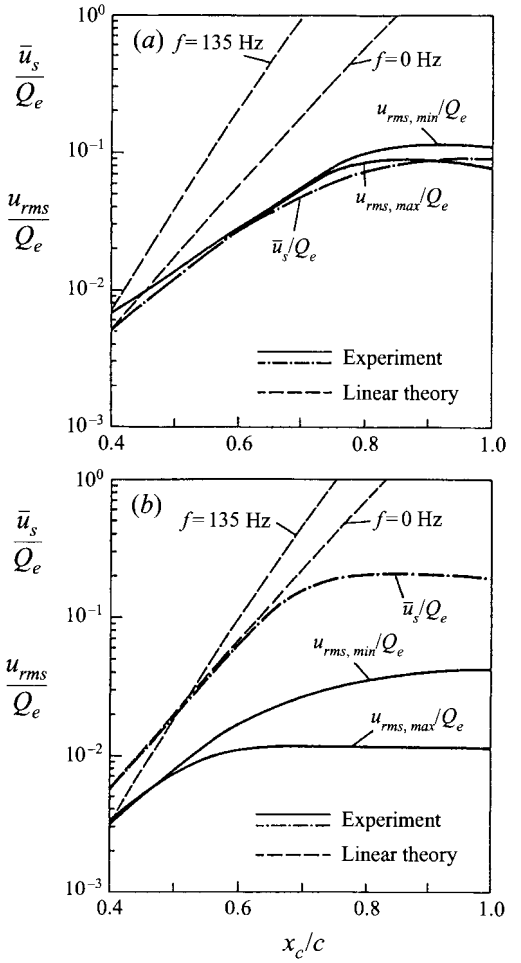

FIGURE 1. Spatial growth of stationary crossflow vortices ($\bar{u}_s$) and travelling waves (u_{rms}) in the two wind tunnels (*a*) 1MK, $Tu = 0.15\%$, and (*b*) NWB, $Tu = 0.08\%$, measured at $Q_{\infty,tun} = 19$ m s^{-1}, $\Phi_{\infty,geo} = 45°$, $\bar{R}_z = 6$ μm.

the formulation of these initial conditions has to be seen as the major issue for future work (see also the review by Saric 1994). It requires knowledge of the disturbance environment and the receptivity. Especially for three-dimensional flows, the solution to this problem still seems to be in an initial state. Investigations should be aimed at establishing physical evidence for the relationship between environmental conditions and the transition process. For this reason, in the present experiments the disturbance development was investigated under varied environmental conditions. These conditions are given by surface roughness, free-stream turbulence, spatial non-uniformities of the oncoming mean flow and sound. Although in this way the receptivity problem cannot be solved directly, it is hoped that the influence of the upstream conditions on the disturbance development and on transition may give some idea of how to model physically relevant initial conditions for non-local nonlinear approaches and to establish data for their validation. It may stimulate activities to incorporate the receptivity into stability analyses. A recent attempt by Bertolotti (1994) on the basis of nonlinear PSE analysis indicates that this may be the procedure to considerably improve the prediction of transition in flows primarily unstable to streamwise vortices.

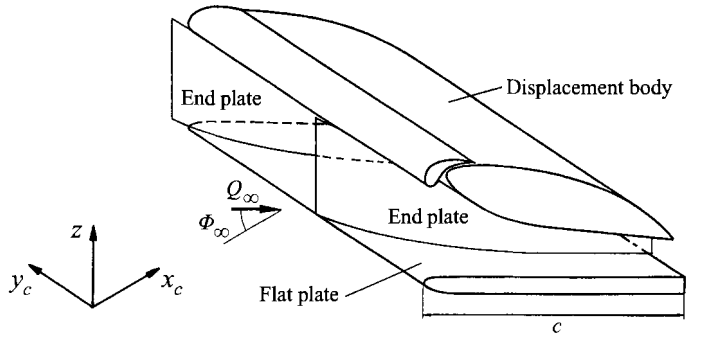

FIGURE 2. Model of the swept flat plate with the displacement body.

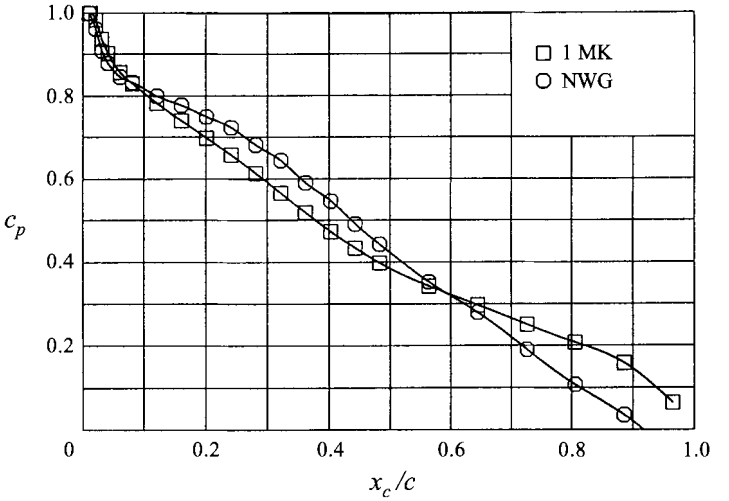

FIGURE 3. Pressure distribution on the swept flat plate in the two wind tunnels 1MK and NWG.

3. Experiment

3.1. *Model and experimental techniques*

In order to reach the objectives discussed in the previous section, a wind-tunnel model with an accelerated three-dimensional boundary layer was required. The quasi-two-dimensional flow on an infinite swept wing represents the most simple case of such a flow. To ensure the dominance of the crossflow instability mechanism, the crossflow Reynolds number generated, $\chi = 1/\nu \int_0^\infty \overline{V}_s \, dz$, should be as large as possible. Other instability mechanisms such as Tollmien–Schlichting (TS) waves or attachment-line instabilities should be damped in the region of amplified crossflow modes. A relatively thick boundary layer and a long laminar flow region are further requirements to facilitate the experimental tracing of the disturbance flow.

Based on these criteria the model of a swept flat plate with the pressure gradient imposed by a displacement body (see figure 2) was designed by Nitschke-Kowsky & Bippes (1988) and further improved by Müller (1990). The chord length of the plate is $c = 500$ mm. Quasi-two-dimensional flow conditions are provided by two end plates shaped according to the curved streamline of the potential flow. The pressure distribution imposed on the plate as measured in two wind tunnels is plotted in figure 3. A nearly constant, negative pressure gradient was obtained with small differences in the two facilities owing to different blockage ratios. This pressure gradient causes the

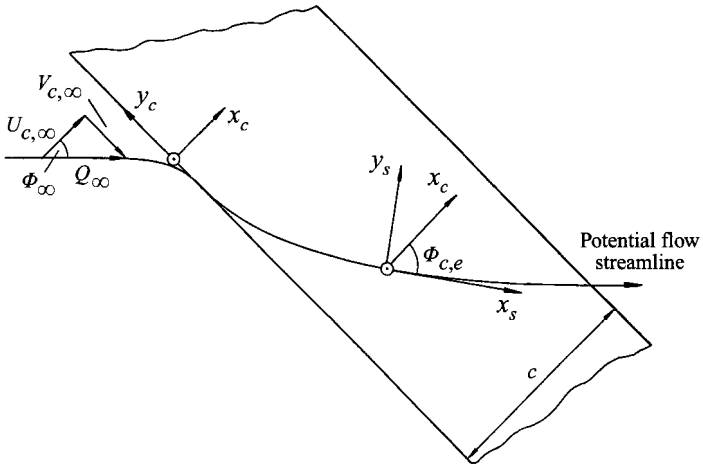

FIGURE 4. Coordinate systems on the swept flat plate.

Facility	Tu (%)	Plate surface	h^+	$Re_{x,tr}$ ($\times 10^5$) ($\gamma = 0.5$)	N_{max}	A_s(0 Hz)
NWB	0.08	Wooden plate (Müller 1990), $\bar{R}_z = 6$ μm	0.27	6.5	14.9	≈ 0.20
1MK	0.15	Plate covered with sandpaper (Müller 1990), $\bar{R}_z = 40$ μm	1.8	6.8	15.5	≈ 0.145
		Roughness elements on polished aluminium plate, $h = 10$ μm	0.45	7.1	16.2	≈ 0.15
		Wooden plate (Müller 1990), $\bar{R}_z = 6$ μm	0.27	7.5	16.9	≈ 0.09
		Aluminium plate, sanded, $\bar{R}_z = 5$ μm	0.23	7.7	17.3	≈ 0.08
		Aluminium plate, polished, $\bar{R}_z = 1.8$ μm	0.081	8.3	18.5	≈ 0.045
1MK/screen	0.27	Aluminium plate, polished, $\bar{R}_z = 1.8$ μm	0.081	7.8	17.5	≈ 0.035
NWG	0.57	Aluminium plate, sanded, $\bar{R}_z = 5$ μm	0.23	5.4	12.3	< 0.01

TABLE 1. Reynolds numbers $Re_{x,tr}$ at 50% intermittency, corresponding N-factors and saturation amplitude A_s(0 Hz) of the stationary crossflow vortices in different wind tunnels and on different plate surface conditions. h^+ was calculated at the location of neutral stability of the stationary vortex mode, N_{max} represents the N-factor of the most amplified (travelling) mode at $x_c/c = 0.9$ from local linear stability calculations using the envelope method (Wagner 1992).

inviscid streamline to be curved as shown in figure 4. Two coordinate systems were used to display the experimental results: the body-fitted system (x_c, y_c, z) and a system fitted with the local direction of the inviscid streamline (x_s, y_s, z). The infinite swept wing conditions yield a constant spanwise velocity $V_{c,e}$ at the outer edge of the boundary layer equal to the spanwise velocity component $V_{c,\infty}$ upstream of the model. Therefore, the local flow angle $\Phi_{c,e}$ depends only on the sweep angle Φ_∞ and the local pressure coefficient c_p. At a geometric sweep angle $\Phi_{\infty,geo} = 45°$ and a wind-tunnel velocity $Q_{\infty,tun} = 19$ m s^{-1}, chosen for most of the tests, crossflow Reynolds numbers $\chi = 160$ could be achieved. Only differences to those conditions are stated explicitly

in the figure captions. The observed maximum momentum thickness Reynolds number $Re_{\delta 2} = 0.404[V_{c,e}^2/(\nu(\mathrm{d}U_{c,e}/\mathrm{d}x_c)_{x_c=0})]^{1/2} = 70$ characterizing the stability of the attachment-line-flow is far below the critical value $Re_{\delta 2,crit} = 230$ (Pfenninger & Bacon 1969, see also Poll 1985). The critical displacement thickness Reynolds number of the TS mechanism at this favourable pressure gradient is $Re_{\delta 1,crit} \approx 10^4$, whereas close to the trailing edge of the plate only $Re_{\delta 1} \approx 10^3$ was obtained. Thus, the disturbance development in this specific boundary-layer flow is purely dominated by crossflow instabilities.

In addition to the previously employed wooden flat plate another model was manufactured from aluminium in order to allow studies of the effect of surface roughness. Both surfaces were coated with varnish and successively sanded and polished to reduce the surface roughness. To obtain quantitative information on the surface roughness, a roughness tester was used. It measured the roughness value R_z defined as a peak-to-peak value averaged from five neighbouring sampling sections (German standard DIN 4768). Those roughness values are generally higher than the frequently used root-mean-square values (Radeztsky *et al.* 1993), for example by a factor of $\sqrt{2}$ for a sinusoidal roughness distribution of constant amplitude. The various surface qualities, given by a spatially averaged value $\bar{R}_z$ (multiple measurements of R_z at different surface locations), are presented together with results of §4 in table 1.

To vary the environmental conditions, the unstable laminar boundary layer was investigated on the identical model in three low-speed wind tunnels. These are the 3.25×2.8 m^2 DLR wind tunnel in Braunschweig (NWB) with an overall turbulence level of $Tu = 0.08\%$ (integrated in the frequency range $2\ \mathrm{Hz} < f < 2$ kHz at free-stream velocities $17 < Q_\infty < 25$ m s^{-1}), and the 1×0.7 m^2 (1MK, $Tu = 0.15\%$) and the 3×3 m^2 (NWG, $Tu = 0.57\%$) DLR wind tunnels in Göttingen. In the 1MK an additional screen could be mounted at the end of the settling chamber which caused the turbulence level to rise to $Tu = 0.27\%$. The stated values of free-stream turbulence levels were obtained accurately by integrating the spectral distribution (see §4.4.1). Differences with turbulence levels presented in Müller (1989, 1990) and Bippes (1991) might be due to different frequencies of the band-pass filters, to their restriction to streamwise fluctuations only and to contamination of the screens. It should be noted that no attempt was made to separate the free-stream velocity fluctuations into vorticity-induced, i.e. in a rotational unsteady velocity field, and sound-induced fluctuations (an irrotational unsteady velocity field). For qualitative comparisons the flow was examined on a similar model made of Plexiglas in the DLR water towing tank (WSG) at Göttingen which provided an environment similar to free flight conditions with negligible turbulence level.

In the wind tunnel experiments, hot-wire anemometry was used for unsteady flow measurements in the boundary layer. Both wall-parallel velocity components $U_s(t)$ and $V_s(t)$ could be obtained with two-wire probes in a V-arrangement. The wires were located in the wall-parallel plane at angles of $+45°$ and $-45°$ to the probe axis. The mean spanwise distance of the wires was ≈ 1.2 mm. The smallest velocity component W_s was not measured. Owing to the strong velocity gradients in the wall-normal direction, V-wire probes are better suited for measurements very close to the wall than X-wire probes whose crossing elements are located at different wall distances. The latter have been used merely for the determination of turbulence levels and of non-uniformities of the mean flow in the test section where strong gradients were not present. The preliminary adjustment of the wall distance of V-wire probes in the boundary-layer measurements was corrected by a linear extrapolation to the wall using measured mean values of the profile in the vicinity of the wall. Possible problems due to a non-parallel

alignment of the V-wire probes to the wall could be overcome by an individual correction of the wall distance of the two wires after the measurement. Further corrections concerning probe vibrations and the influence of spanwise velocity gradients on the measurement were applied if necessary (Deyhle 1993).

For measurements on the model and in the test section the traversing mechanism of the hot-wire probes was controlled by an acquisition computer allowing fully automatic measurements at preselected spatial positions. An eight-channel 12 bit A/D-converter allowed the acquisition of hot-wire, pressure and temperature signals sampled for boundary-layer measurements at a frequency of $f_s = 3.8$ kHz for a period of $\bar{t} = 6.3$ s. These values cover the whole band of unstable non-stationary instability modes occurring at the present flow conditions. Larger averaging times or higher sample frequencies did not lead to significant improvement. The hot wires were calibrated for velocity and flow angle. The measured temperature-compensated velocities are displayed in the inviscid streamline coordinate system. To evaluate power spectra, a FFT algorithm with Hanning window function was used and typically 11 spectra of 2^{11} samples were averaged.

The region on the model where the disturbances are of measurable size at the chosen free-stream conditions starts at $x_c/c \approx 0.4$. To determine the characteristics of the disturbance flow, eight profiles per vortex wavelength were measured over two to three vortices, and to determine the disturbance growth up to the first appearance of turbulence spots, measurements were performed at six streamwise locations. Thus fluctuating velocity signals were measured at more than two thousand spatial positions for one specific disturbance environment.

To investigate the linear growth of disturbances more precisely, attempts have been made to introduce artificially well-defined disturbances into the boundary layer and to observe their growth. Up to now this could be achieved successfully merely for the stationary crossflow vortices. As a trial, local heating elements at $x_c/c \approx 14\%$ chord were used to stimulate these vortices (see Bippes 1991). However, the tiny roughness elements on the smooth surface of the plate employed by Saric (1992) turned out to be an easier method for this purpose. The roughness elements used in the present work were dots and stripes from transfer sheets with a height of $h = 10 \pm 1$ μm. In the leading-edge region this physical height corresponds to a very small value in non-dimensional wall units of $h^+ = u_\tau h/\nu \approx 0.45$ or a roughness Reynolds number of $Re_h = h\bar{U}_s(h)/\nu \approx 0.2$. Further experimental results are given in Bertolotti & Bippes (1994). The surface conditions could be changed by means of roughness elements in the present work also.

In order to change the acoustic environment in the 1MK, experiments were performed with sound waves introduced into the oncoming flow. For this purpose a loudspeaker was placed with its diaphragm parallel to the wall of the settling chamber producing plane sound waves in the test section at frequencies up to $f \approx 140$ Hz without disturbing the test section flow. Driven by a hifi-power amplifier, sound pressure levels up to SPL ≈ 111 dB (reference pressure 20 μPa) were obtained for a sinusoidal excitation in the frequency range of travelling instability modes. The propagation direction and the SPL of the sound waves were checked by correlation measurements with microphones.

3.2. *Boundary-layer base flow*

In this section the boundary-layer base flow on the swept flat plate model is documented and compared with infinite swept wing boundary-layer calculations which are the basis of the stability analyses of Meyer (1989) and Wagner (1992). The potential flow is accelerated over the whole plate owing to the negative pressure gradient (figure 3).

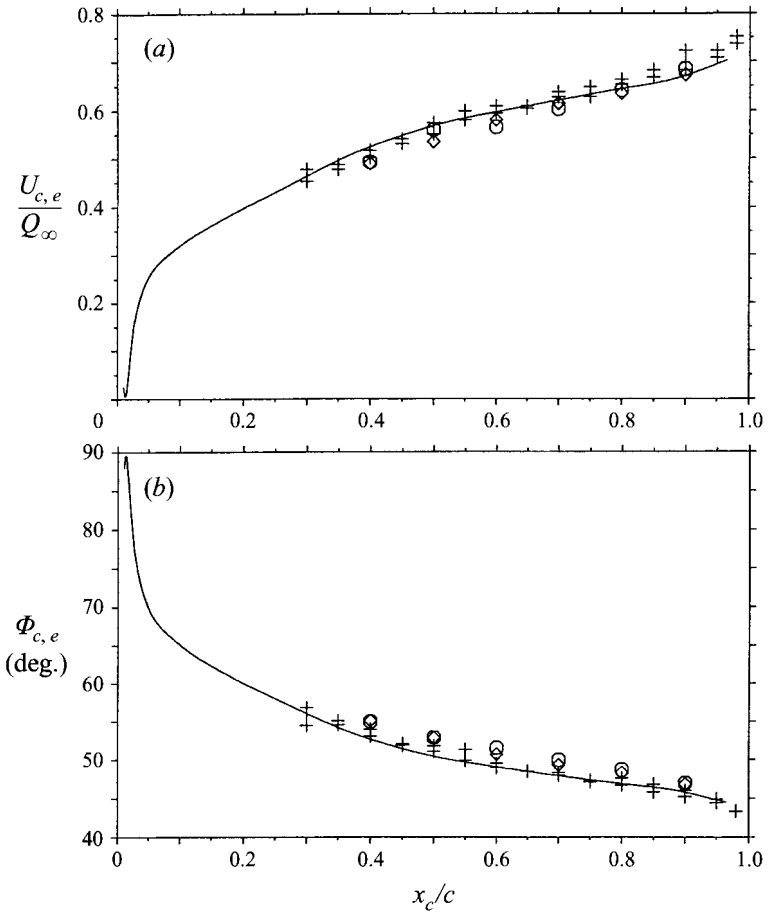

FIGURE 5. Streamwise distribution of (*a*) mean velocity $U_{c,e}$ and (*b*) local flow angle $\Phi_{c,e}$ at the outer edge of the boundary layer. ○, ◇, +, Hot-wire measurements at different test runs; ——, calculated from the measured pressure distribution using the assumption of infinite swept wing conditions with $Q_\infty = 20.5$ m s^{-1}, $\Phi_\infty = 43.5°$.

The velocity distribution $U_{c,e}(x_c)$ outside of the boundary layer is plotted in figure 5(*a*). The symbols denote hot-wire measurements for different test runs, indicating the reproducibility of the model adjustment in the wind tunnel. The solid line represents the velocity distribution calculated from the measured pressure distribution in the 1MK with the assumptions of infinite swept wing flow. In order to fit the two curves, the free-stream velocity Q_∞ and the sweep angle Φ_∞ had to be slightly modified. The reasons are both deviations from the nominal wind-tunnel velocity $Q_{\infty,tun}$ and from the geometrical sweep angle $\Phi_{\infty,geo}$, especially with increasing blockage ratio of the facility, and problems with the simulation of infinite swept wing conditions by means of the end plates. The best fit was found for $Q_\infty = 20.5$ m s^{-1} and $\Phi_\infty = 43.5°$ compared with $Q_{\infty,tun} = 19$ m s^{-1} and $\Phi_{\infty,geo} = 45°$. These fitted values were used for the stability calculations as well as for the determination of transition Reynolds numbers in §4.5. In figure 5(*b*) the distribution of the local flow angle $\Phi_{c,e}$ is displayed. The values calculated from the pressure measurement using the best-fit values of Q_∞ and Φ_∞ also compare well with the hot-wire measurement. The measured spanwise velocity $V_{c,e}$ shows a spanwise variation of less than 6% from the nominal value $V_{c,e} = Q_\infty \sin \Phi_\infty$ which is constant in the x_c-direction.

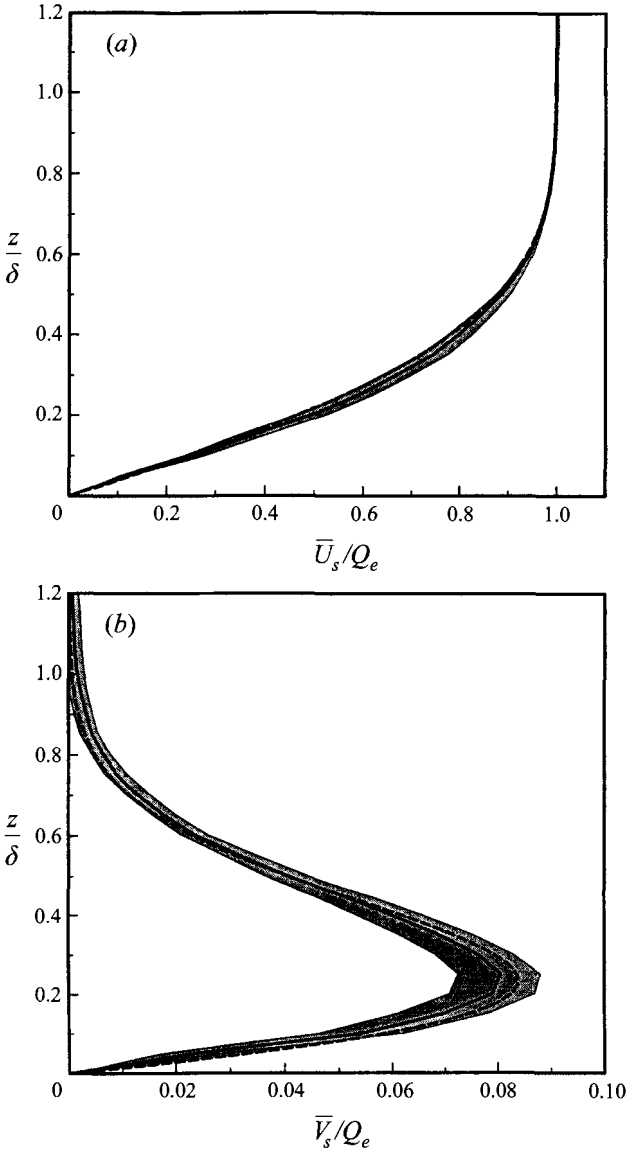

FIGURE 6. Comparison of measured and calculated mean velocity profiles (*a*) $\bar{U}_s(z)$ and (*b*) $\bar{V}_s(z)$ in the boundary layer at $x_c/c = 0.4$. The shaded areas denote the spanwise variation of measured profiles $\bar{U}_s$, $\bar{V}_s$ due to the stationary crossflow vortices; ——, spanwise averaged mean velocity profiles $\overline{\bar{U}}_s$, $\overline{\bar{V}}_s$; – – – –, calculation (measurement at $Tu = 0.15\%$, $\bar{R}_z = 1.8$ μm, artificial roughness elements $d_h = 3.3$ mm, $h = 10$ μm, $\Delta y_c = 11.1$ mm at $x_c/c = 0.08$).

In figure 6 the boundary-layer profiles from experiment and calculation are compared at a streamwise position $x_c/c = 0.4$. At this location nonlinear interaction between base flow and stationary disturbance flow is sufficiently small. Therefore, comparisons between measured boundary-layer mean flow and calculated base flow are restricted to this region. The spanwise variation of measured profiles deformed by the crossflow vortices is indicated in this figure by the shaded area. In order to facilitate the comparison with calculations the measured mean velocity profiles $\bar{U}_s$, $\bar{V}_s$ were averaged in the spanwise direction y_c. This is denoted by $\overline{\bar{U}}_s$, $\overline{\bar{V}}_s$ and plotted as solid lines in figure 6(*a*, *b*). In the linear range of amplification, $\overline{\bar{U}}_s$ and $\overline{\bar{V}}_s$ represent the base flow

x_c/c	δ (mm)	δ_1 (mm)	χ
0.2	1.98	0.52	60
0.3	2.21	0.56	81
0.4	2.37	0.60	97
0.5	2.56	0.65	107
0.6	2.76	0.70	114
0.7	2.91	0.74	123
0.8	3.00	0.75	136
0.9	3.05	0.74	149
0.98	3.07	0.73	159

TABLE 2. Boundary-layer thickness δ (99.9% of $\bar{U}_s$), displacement thickness δ_1 of the $\bar{U}_s$ profiles and crossflow Reynolds numbers χ of the calculated base flow at $Q_\infty = 20.5$ m s^{-1}, $\Phi_\infty = 43.5°$.

profiles. The agreement with the calculation, given by the dashed lines, is considered to be satisfactory. To conclude the description of the base flow, the integral quantities used for non-dimensionalizing the results such as boundary-layer thickness δ, displacement thickness δ_1, and crossflow Reynolds number χ are given in table 2.

4. Results and discussion

The dependence of the transition process upon the upstream conditions manifests itself in a change of the complex unsteady three-dimensional disturbance motion in the nonlinear range of amplification. For the interpretation of the observations it is necessary to first characterize the instability modes, their initial development as well as typical nonlinear structures and to compare them with results of theoretical approaches.

4.1. *Identification of instability modes*

A first insight into the main features of the disturbance motion developing within the investigated unstable three-dimensional boundary layer is given in figure 7. It shows a result of the unsteady flow field measurements described in §3.1. Velocities are displayed in components aligned with the inviscid streamlines coordinate system (x_s, y_s, z) and plotted versus the model fixed coordinates y_c, z for constant chord positions x_c/c. For a more illustrative presentation, the data acquired on a non-equidistant 19×23 measurement grid were spline interpolated first in the z-, then in the y_c-direction to a 40×40 grid. The mean crossflow velocity $\bar{V}_s = \overline{\bar{V}_s} + \bar{v}_s$ as measured at $Tu = 0.27\%$ and $\bar{R}_z = 5$ µm is shown on the left-hand side of figure 7. It is composed of the base flow component $\overline{\bar{V}_s}$ and a stationary disturbance component $\bar{v}_s$. At $x_c/c = 0.4$ (figure 7*a*) the mean crossflow velocity profiles $\bar{V}_s$ are just becoming affected by a spanwise-periodic stationary disturbance $\bar{v}_s$. In the downstream direction this disturbance is amplified and leads to a considerable distortion of the mean crossflow profiles.

For a clear identification of unsteady modes the crossflow root-mean-square value (r.m.s. value) v_{rms} has been displayed on the right-hand side of figure 7. The crossflow instead of the streamwise component is considered because, at positions further upstream, the model geometry requires a long probe holder which reduces the holder stiffness and contaminates the hot-wire signal by probe vibrations. In this case v_{rms} is less affected than u_{rms} because the analysis of two-wire probe signals cancels out the vibrational portion in the crosswise r.m.s. value but increases the streamwise value. It should be noted, however, that the situation changes further downstream. There shorter probe holders give a reduction of the vibrational content which can be

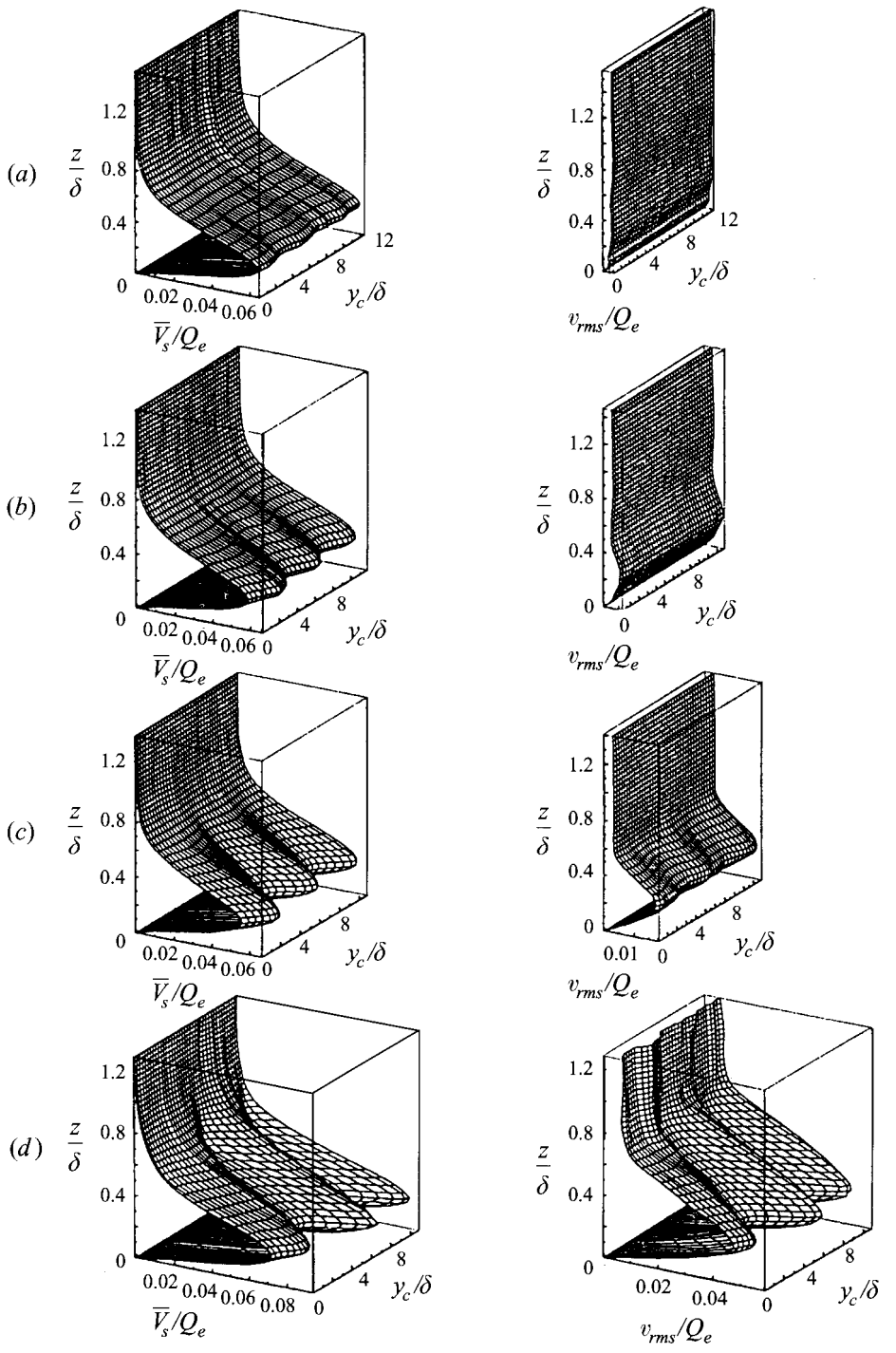

FIGURE 7. Streamwise development of the time-averaged crossflow velocity $\overline{V}_s$ (left-hand side) and the r.m.s. value v_{rms} of crossflow fluctuations (right-hand side) in the unstable boundary layer (Tu = 0.27%, $\bar{R}_z = 5$ μm). (*a*) $x_c/c = 0.4$; (*b*) $x_c/c = 0.5$; (*c*) $x_c/c = 0.6$; (*d*) $x_c/c = 0.9$.

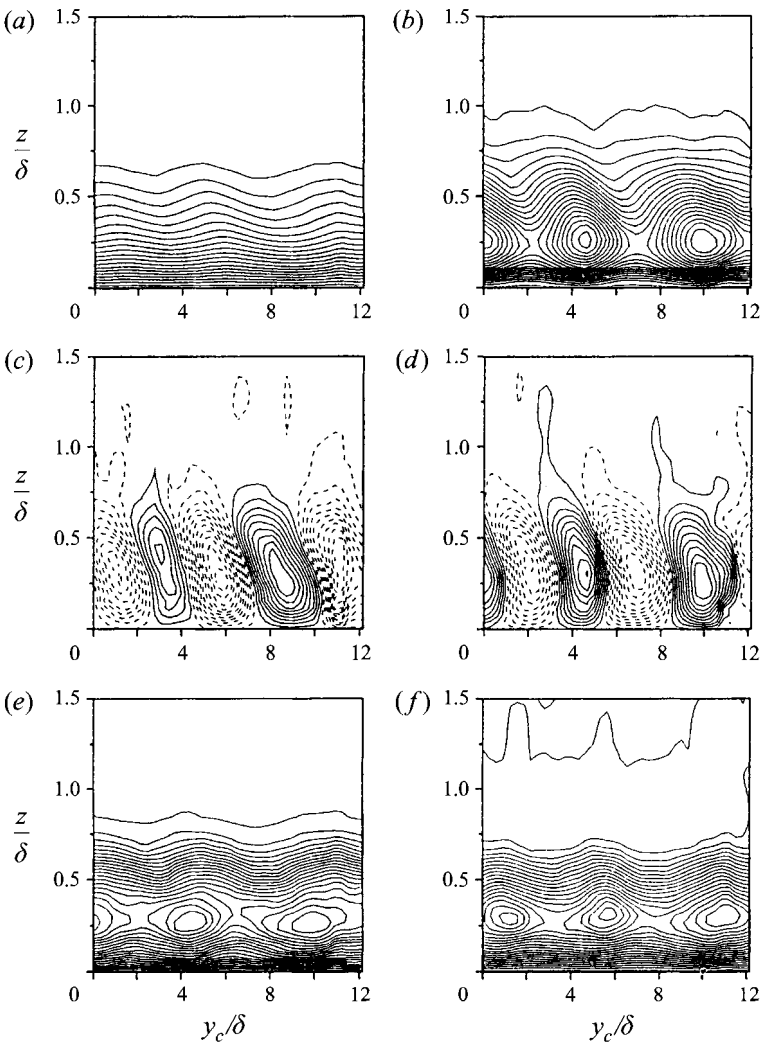

FIGURE 8. Isolines of (*a*) the mean velocity $\bar{U}_s$ and (*b*) $\bar{V}_s$; (*c*) the stationary disturbances $\bar{u}_s$ and (*d*) $\bar{v}_s$; (*e*) the r.m.s. values of fluctuations u_{rms} and (*f*) v_{rms} in the (y_c, z)-plane at $x_c/c = 0.7$, $Tu = 0.27\%$, $R_z = 5$ μm.

neglected compared with higher disturbance amplitudes. Additionally, owing to increasing spanwise gradients of the mean flow, the evaluation of the crosswise velocity components becomes less accurate. In this situation, an interpretation of results is better based on streamwise r.m.s. values. As can be seen in figure 7(*a*), the crossflow r.m.s. fluctuations in the boundary layer at $x_c/c = 0.4$ are still smaller than the free-stream value with a small maximum at a wall distance of $z \approx \delta/4$. The increase in v_{rms} in the downstream direction indicates that in the boundary layer investigated here not only the steady disturbance modes but also the unsteady modes develop. In addition, at $x_c/c = 0.6$ (figure 7*c*) the spanwise distribution starts to be deformed periodically. At $x_c/c = 0.9$, the maximum in the v_{rms}-distribution has decreased slightly compared to more upstream locations, but the shape function has become wider in the wall-normal direction.

A closer insight into the structure of the disturbances is provided in figure 8, which shows the distributions of the streamwise and spanwise velocities by means of isotachs

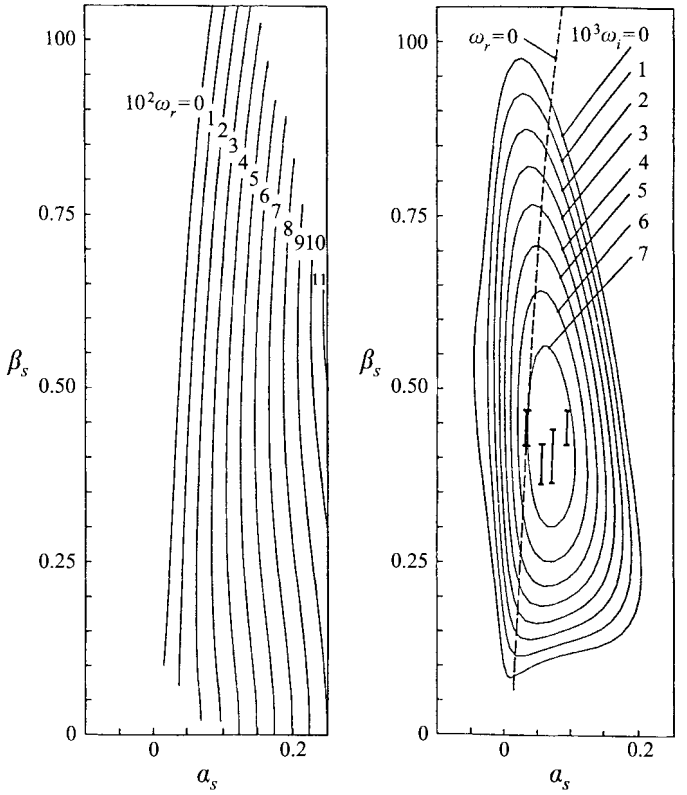

FIGURE 9. Stability diagram of local linear theory for the swept flat plate boundary layer at $x_c/c = 0.8$, $Q_\infty = 19\ \mathrm{m\ s^{-1}}$, $\Phi_\infty = 45°$ (Meyer 1989). α_s, β_s are the components of the wavenumber vector; ω_r is the frequency of the disturbances; ω_i is the temporal amplification rate. Experimental results are given by bars for the stationary crossflow-vortex mode (obtained in different environments) and for three travelling modes ($f = 60$, 100, 140 Hz, corresponding to $\omega_r = 0.014$, 0.024, 0.033, with propagation directions as identified by Deyhle *et al.* 1993).

in an (y_c, z)-plane at $x_c/c = 0.7$. Figure 8(a, b) demonstrates again the periodic spanwise deformation of the mean flow under the action of the steady disturbances. The crossflow component $\bar{V}_s$ in figure 8(b) indicates the structure of corotating vortices known from flow visualizations. The structure of the steady disturbances themselves is obtained by subtracting the spanwise-averaged mean flow $\overline{\bar{U}}_s$, $\overline{\bar{V}}_s$ from the mean flow $\bar{U}_s$, $\bar{V}_s$. According to figure 8(c, d) the steady crossflow modes are counter-rotating vortices corresponding to the normal mode solutions of linear stability theory. In figure 8(e, f) the r.m.s. content of the velocity field is shown. Although it gives no further information on the nature of this unsteady instability, it should be noted that according to linear stability theory no spanwise variation but horizontal isolines would be expected. The variation starts, for the present upstream conditions, at $x_c/c = 0.6$ (compare figure 7) and is always observed as soon as the stationary vortices become of clearly measurable size. The reason leading to this effect is discussed in §4.3.

Further characteristics of the unsteady modes may be inferred from previous measurements. The typical spectral distribution of the velocity fluctuations (given in figure 9*b* of Bippes *et al.* 1991) shows a band of amplified frequencies up to $f \approx$ 500 Hz with a rather flat maximum in this specific case around $f = 90$ Hz. That figure also shows calculated temporal amplification rates of the most-amplified travelling modes in the various propagation directions. Their envelope reveals good agreement

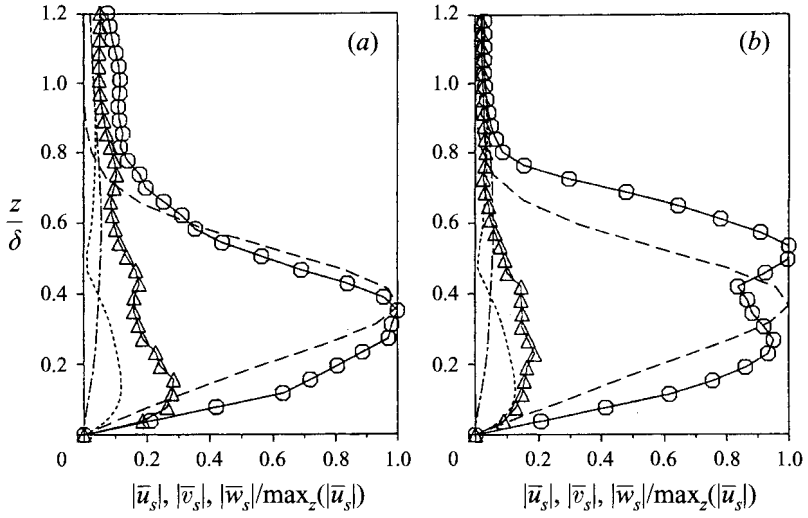

FIGURE 10. Amplitude functions of the stationary instability mode at two streamwise positions (*a*) $x_c/c = 0.6$ and (*b*) $x_c/c = 0.8$. Experiment: ○, $|\bar{u}_s|$; △, $|\bar{v}_s|$ ($Tu = 0.15\%$, $\bar{R}_z = 5$ μm); local linear theory: ——, $|\bar{u}_s|$; · · · · · ·, $|\bar{v}_s|$; - - - - - - - -, $|\bar{w}_s|$.

with the shape of the measured spectrum, i.e. with the most-amplified travelling modes observed in the tests. Additional measurements of wavelength, phase velocity, and propagation direction (for detailed description see Deyhle *et al.* 1993) showed further agreement with linear theory.

In order to compare the experimentally identified instability modes with the most-amplified modes of temporal linear theory, measured wavenumbers are displayed in the stability diagram calculated by Meyer (1989) at a streamwise position $x_c/c = 0.8$ (figure 9). On the right-hand side, lines of constant temporal amplification ω_i, are plotted in the real wavenumber plane α_s, β_s and on the left-hand side the lines of constant frequency ω_r. Overlaying both diagrams shows that the most-amplified stationary vortices ($\omega_r = 0$) are closely aligned with the inviscid streamline whereas the wavenumber vectors of the most-amplified travelling modes point in different directions depending on the frequency. For the very low frequencies the wavenumbers (α_s, β_s) are roughly the same as those for the zero-frequency mode. However α_s increases with increasing frequency. This dependence was also found in experiments. The bars plotted on the right-hand side of figure 9 represent measured stationary and travelling modes, the latter of three different frequencies. Their wavenumbers are all located in the calculated region of strongest amplification revealing a very good agreement with theory.

An additional comparison was made for the amplitude functions of the steady modes. They were calculated from the hot-wire measurements as $|\bar{u}_s|(z) = \max_{y_c}|\bar{U}_s(y_c, z) - \overline{\bar{U}}_s(z)|$ and $|\bar{v}_s|(z) = \max_{y_c}|\bar{V}_s(y_c, z) - \overline{\bar{V}}_s(z)|$. In figure 10 they are compared with the eigenfunctions of linear theory for two specific streamwise locations. At $x_c/c = 0.6$ (figure 10*a*) there is still fair agreement between theory and experiment. However, small differences exist concerning the location above the wall of the maximum amplitude of the streamwise amplitude function. Discrepancies in the amplitude of the $\bar{v}_s$-functions were attributed to measurement uncertainties due to the influence of the spanwise velocity gradients on the crossflow component V_s (Deyhle 1993). Further downstream at $x_c/c = 0.8$ (figure 10*b*) where nonlinear effects are obvious (§4.3), the shape of the $\bar{u}_s$-amplitude function differs considerably from linear theory. A second

local maximum occurs in the experiment, which thickens the shape in the wall-normal direction. The comparison of the amplitude functions of the non-stationary modes with theory shows similar behaviour with increasing streamwise position (Müller 1990).

Hence it can be stated that the stationary as well as non-stationary instabilities identified in the experiment on the swept flat plate agree with the most amplified modes predicted by linear theory.

4.2. *Disturbance growth*

The disturbance growth measured by Müller (1990) in previous experiments is considerably smaller than predicted by linear theory (figure 1). In §2 it was argued that this may be due to nonlinear effects. In order to provide more realistic data on the linear disturbance growth an attempt has been made to repeat Müller's measurements at a reduced free-stream velocity, $Q_{\infty,tun} = 10$ m s^{-1} instead of 19 m s^{-1}. This enables the tests to be carried out closer to the neutral stability conditions where nonlinear effects should be less significant. However, it must be kept in mind that under natural conditions of transition the disturbance motion comprises a band of instabilities initiated at amplitudes and frequencies varying in space and time. In most cases this results in an irregular disturbance motion. Individual unsteady disturbances cannot be identified and traced in the downstream direction. Therefore, reliable comparison with theoretical approaches and conclusive interpretations and statements of general meaning are handicapped. The well-established remedy to overcome this limitation is the controlled excitation of the instabilities, the ingenious contribution to experimental transition research by Schubauer & Skramstad (1948). However, in the case of crossflow instability, where the instability waves propagate at angles between 50° and 90° to the inviscid flow, the conventional vibrating ribbon technique cannot be applied. Advanced techniques as used by Liepmann, Brown & Nosenchuck (1982) or Corke & Mangano (1989) to stimulate three-dimensional waves in two-dimensional flows can be applied to flows unstable to crossflow instability only if any three-dimensional surface protuberance is avoided which in turn would initiate stationary crossflow vortices. It will be shown in §4.4.4 that three-dimensional surface roughness of height less than one dimensionless wall unit may trigger streamwise vortex instabilities. For this reason, to date only stationary instability modes could be stimulated artificially. It should be noted, however, that an advanced technique allows this problem to be overcome as shown in the later experiment of Lerche & Bippes (1995). The techniques used in the present study are described in §3.1.

For precise measurements of the steady modes with hot-wire anemometry, the amplitudes should not be much smaller than 0.5% of the undisturbed flow. In our case this required the stimulation of the steady modes at values considerably larger than those of the free-stream velocity fluctuations which stimulated the unsteady modes. Figure 11 shows the result obtained for the steady mode excited at a wavelength close to the most unstable one (according to local linear theory the most unstable wavelength on the swept flat plate varies only very weakly in the downstream direction, Bippes *et al.* 1991). The difference to figure 1 is obvious. Now, there is no evidence of the beginning of saturation in the disturbance growth up to the most downstream measurement. For comparison with local linear theory, the growth calculated for the stimulated steady mode and the most-amplified travelling modes (now u_{rms} denotes the summation over four modes in the frequency range $25 < f < 100$ Hz) is also displayed in figure 11. Since the growth of single travelling modes determined from the power spectrum is only slightly larger than the growth of the r.m.s. fluctuations over the whole band of frequencies (as has been shown by Müller 1989), it can be stated that now, in

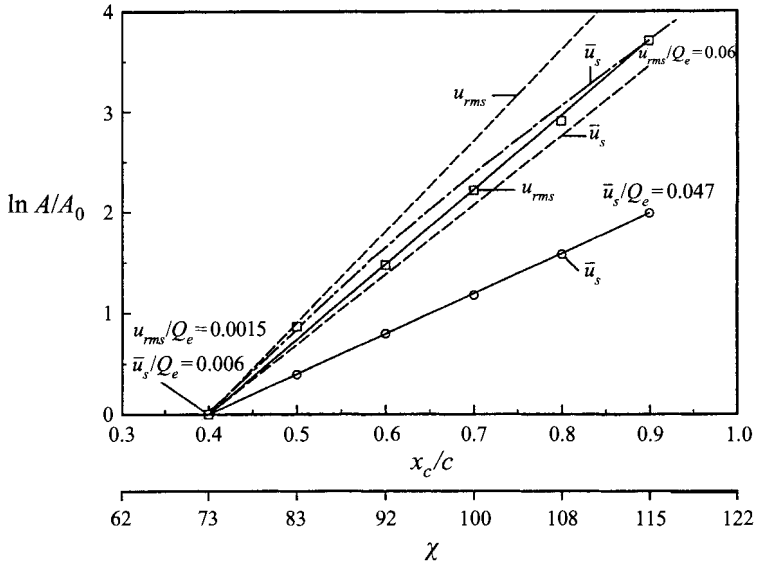

FIGURE 11. Spatial growth of stationary ($\bar{u}_s$) and non-stationary (u_{rms}) instability modes in the 1MK ($Tu = 0.15\%$) at $Q_{\infty,tun} = 10$ m s^{-1} with artificially stimulated crossflow vortices of wavelength $\lambda_c = 17.9$ mm at $x_c/c = 0.14$ using local wall heating. $\bar{u}_s$, u_{rms} denote the local maximum of the disturbance functions. Experiment: ○, □; local linear theory: ———; non-local linear theory: ·····.

contrast to the results in figure 1, the travelling modes are more amplified than the stationary modes as expected from local linear theory. Nevertheless, the growth of both modes is still overpredicted. One of the reasons for this discrepancy may be seen in the weakness of local linear theory for boundary-layer flows unstable to streamwise vortices as with the Görtler problem (Hall 1983). However, the non-local linear growth of the stimulated steady mode calculated with Bertolotti's code (Bertolotti 1995, personal communication) predicts an even higher amplification than local theory (see figure 11). Another reason may be found in an early nonlinear development due to disturbance interaction and to the mean flow distortion by the stationary vortices even though a distinct difference between maximum and minimum r.m.s. fluctuations associated with a spanwise periodic variation of the unsteady disturbance amplitudes has not yet become obvious. In the next section these aspects will be elucidated in more detail.

4.3. *Nonlinear effects*

First hints of the appearance of nonlinear developments which may lead to specific features of the disturbance growth as in figure 1 may be found in figures 7 and 8. Comparing the downstream development of the mean flow and the r.m.s. fluctuations (figure 7), it becomes obvious that, besides the spanwise periodic distortion of the mean flow which is due to the stationary vortices, a periodic spanwise variation of the r.m.s. profiles also occurs. In all our tests, this variation could only be observed in the presence of stationary vortices. Moreover, its wavelength corresponds to that of the stationary vortices (compare figures 8*c*, *d* and *e*, *f*). This implies that this feature is due to an interaction between the steady and unsteady disturbance modes. In our experiment it could first be identified at amplitudes $\bar{u}_s/Q_e = 0.01$–0.02 of the stationary vortices. At a surface roughness $\bar{R}_z = 5\,\mu$m and $Tu = 0.27\%$, where the growth of steady modes is attenuated by a higher initial amplitude of travelling modes, these conditions are achieved at $x_c/c = 0.5$–0.6 (figure 7). At lower free-stream turbulence (figure 1*b*) this occurs even earlier.

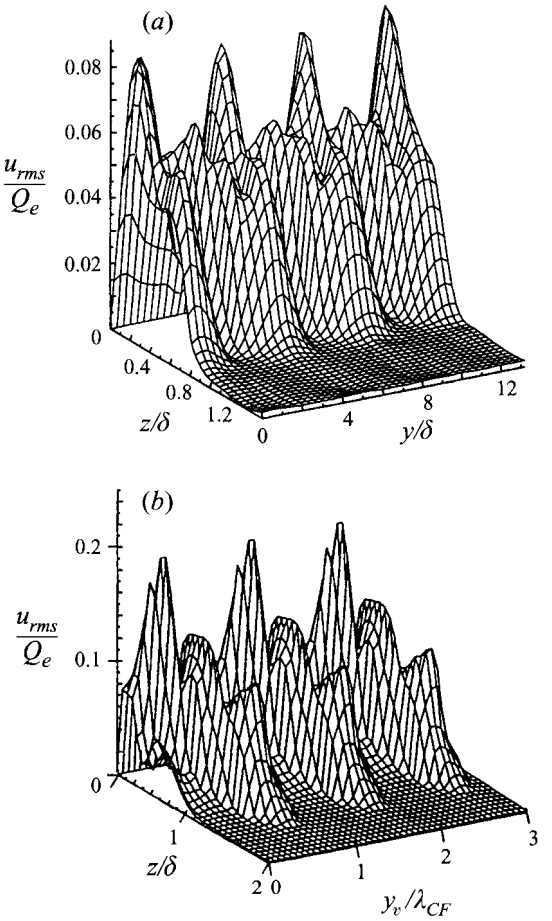

FIGURE 12. Comparison of the streamwise fluctuations (r.m.s. values u_{rms}) from (*a*) experiment and (*b*) direct numerical simulation of Wagner (1992). The index v denotes crossflow-vortex-fitted coordinates. λ_{CF} is the wavelength of the primary stationary vortex considered in the DNS.

In the DNS analyses of Wagner (1992) and Müller *et al.* (1994), as well as in the nonlinear PSE analysis of Malik & Chang (1994), the same phenomenon is predicted as being due to additional Fourier modes generated from interaction between a primary steady and unsteady modes. This is illustrated in figure 12 which compares the spanwise variation of the r.m.s. profiles obtained in the DNS analysis by Wagner (1992) with the present experiment. The qualitative agreement is evident. It should be pointed out that a quantitative comparison would require the correct adaptation of the initial perturbations for the DNS analysis to those of the experiment at the location of neutral stability. The initial perturbations result from the environmental disturbances and the receptivity mechanisms. In most cases the former will be very small and beyond the limits of precise measurements, i.e. they have to be modelled by empirical means. The latter are more or less unknown. Hence, no such attempt has been made up to date. It is proposed to first include the receptivity in a PSE analysis so that only the environmental disturbance content has to be determined or modelled. A preliminary study has been carried out by Bertolotti & Bippes (1994). The present experiments described in §4.4 are aimed at contributing further to the knowledge on the influence of the environmental disturbances in order to give some hints for better modelling of initial conditions.

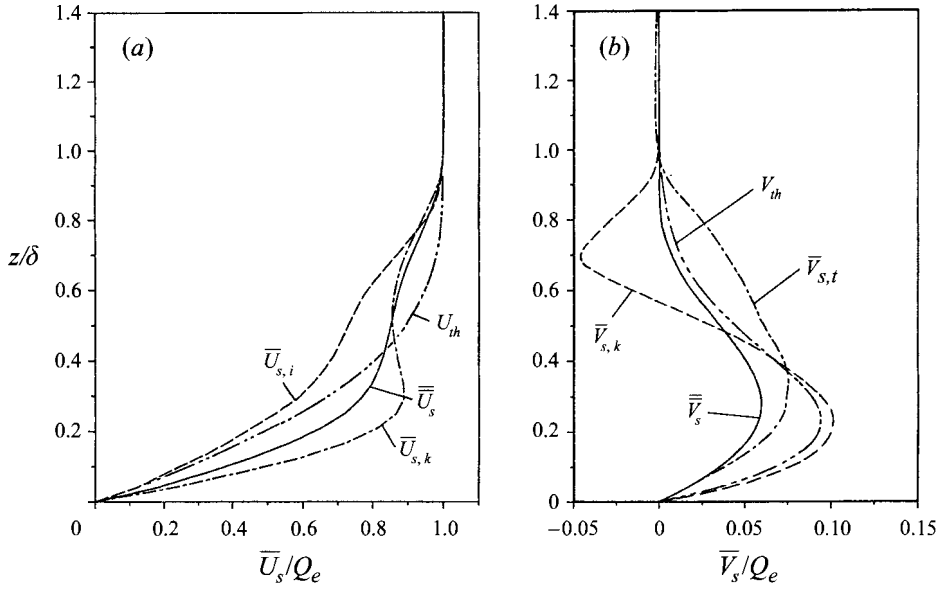

FIGURE 13. Deformation of (*a*) the streamwise $\bar{U}_s$ and (*b*) the crossflow velocity component $\bar{V}_s$ of the mean flow caused by the stationary disturbances. $\bar{U}_{s,i}$, $\bar{U}_{s,k}$, $\bar{V}_{s,i}$, $\bar{V}_{s,k}$ are selected profiles, measured at different spanwise positions y_c; $\bar{\bar{U}}_s$, $\bar{\bar{V}}_s$ are spanwise-averaged profiles from experiment; U_{th}, V_{th} are base flow profiles from laminar boundary-layer calculations using the pressure distribution from experiment (measurement in the 1MK, $Tu = 0.15\%$, taken at $x_c/c = 0.85$ on the polished aluminium plate, $\bar{R}_z = 1.8$ μm, with artificial roughness elements $d_h = 3.3$ mm, $h = 10$ μm, $\Delta y_c = 11.1$ mm located at $x_c/c = 0.08$).

When considering the nonlinear developments it has to be taken into account that, as in all boundary-layer flows primarily unstable to stationary vortices, the base flow becomes distorted so that the stability characteristics are changed. In the present case, this distortion becomes most evident in figure 7 where a sequence of mean flow profiles measured at subsequent downstream locations is shown. Such a distortion was taken into account in the secondary stability analysis by Fischer & Dallmann (1991). They obtained secondary instabilities which also lead to the spanwise variation of the r.m.s. fluctuations as in the DNS and PSE analyses. Moreover, they predicted the splitting of the growth of the unsteady modes if measured along the streamwise zones of maximum and minimum velocity $\bar{U}_s$, $\bar{V}_s$ (figure 1). According to their analysis this development starts at very small amplitudes of the primary steady modes in agreement with our experiment. Further downstream the mean flow distortion leads to inflectional mean flow profiles for both the streamwise and spanwise components $\bar{U}_{s,i}$, $\bar{V}_{s,i}$ as displayed in figure 13. Even the spanwise-averaged mean flow profiles $\bar{\bar{U}}_s$, $\bar{\bar{V}}_s$ no longer compare with the laminar boundary layer profiles U_{th}, V_{th} on which linear theory is based. In the DNS and nonlinear PSE analyses by Meyer & Kleiser (1989) and Malik & Chang (1994), respectively, as well as in the secondary stability analysis by Fischer & Dallmann (1991) such a deformation of the base flow is explained as nonlinear interaction between the instabilities and the base flow. The profiles $\bar{U}_{s,i}$, $\bar{V}_{s,i}$ selected within a period of the spanwise mean flow variation demonstrate that locally the mean flow is even more deformed than $\bar{\bar{U}}_s$, $\bar{\bar{V}}_s$ (figure 13). Thus it becomes evident that the streamwise vortices as the primary instability give rise to various forms of secondary instabilities; indeed, in their secondary stability analysis of our experiment, Fischer, Hein & Dallmann (1993) obtained not only the spanwise variation of the r.m.s.

fluctuations, but also a high-frequency mode for amplitudes of the primary steady mode larger than 10% of the local inviscid flow. A similar result is reported by Malik & Chang (1994). They predicted the appearance of a strongly amplified secondary high-frequency mode in swept Hiemenz flow for amplitudes larger than 17%. High-frequency modes were observed experimentally by Poll (1985) on a swept cylinder and by Kohama, Saric & Hoos (1991) on a swept wing. In our experiment the high-frequency mode was found only immediately prior to transition. It will be discussed in more detail in §4.5.

The conclusion of these observations is that the development of the disturbance motion in the presence of crossflow instability is characterized by an early nonlinear development which obviously depends on the initial conditions. In the following those dependencies are studied in detail.

4.4. *Variation of initial conditions*

The experiments with the identical model in different facilities revealed rather distinct developments of stationary and non-stationary instability modes, i.e. different transition processes. As already pointed out, the reason for this behaviour is differences in the environmental conditions. However, the relevant content of environmental disturbances is still unknown for three-dimensional boundary layers. The key problem is the receptivity of the flow to these environmental disturbances and hence their conversion into instability modes. While no reliable receptivity theory is available, the experiment can only try to identify effective environmental disturbances and study their influence on the development of the instabilities. The main difficulty to overcome is the fact that free-stream disturbances in wind tunnels cannot be varied individually; they are intrinsically coupled. A strategy of examining the transition processes in different test facilities with overlapping parameter ranges (Morkovin & Reshotko 1989) seems to be the only way to gain knowledge of the transition problem to improve prediction.

A variety of these external disturbances has to be examined. For the present work four environmental conditions were considered: free-stream turbulence, sound, mean flow inhomogeneities and surface roughness. Their variation and the corresponding dependence of the disturbance development in the boundary layer are described in the following sections.

4.4.1. *Free-stream turbulence*

It has already been shown in §2 that the disturbance development in two different wind tunnels, characterized by turbulence levels of $Tu = 0.08\%$ and 0.15%, exhibits remarkable differences. Turbulence level is not the only, but it is the most obvious, difference between those tunnels. Hence, as a first step to elucidate possible dependences of the disturbance development on Tu and to support the previous results, the free-stream turbulence was varied further. In the 1MK wind tunnel an additional coarse screen was mounted very close to the contraction which allowed investigations at $Tu = 0.27\%$, while in the NWG wind tunnel experiments could be performed at $Tu = 0.57\%$. In both environments the development of stationary and travelling instability modes was measured. The results are compared with previous results obtained in the 1MK at $Tu = 0.15\%$ and in the NWB at $Tu = 0.08\%$.

To determine experimentally the growth in figures 1 and 11, the maxima of the amplitude functions $|\overline{u}_s|(z), u_{rms}(z)$ were used. However, from figure 10 it becomes obvious that this method can describe the growth of disturbances only in the early stages. Further downstream the measured shape of amplitude functions differs strongly

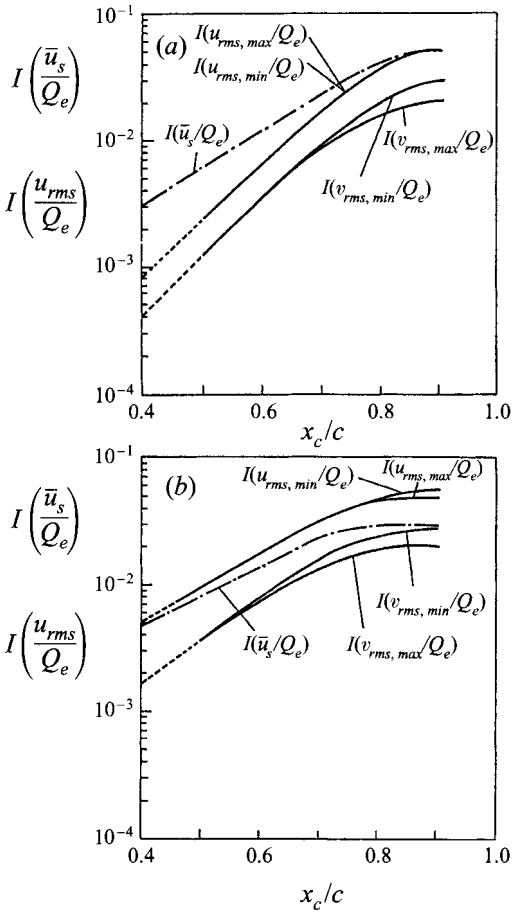

FIGURE 14. Spatial growth of stationary ($\bar{u}_s$) and non-stationary (u_{rms}, v_{rms}) instability modes in the 1MK (*a*) without ($Tu = 0.15\%$) and (*b*) with the additional screen ($Tu = 0.27\%$) at $Q_{\infty,tun} =$ 19 m s^{-1}, $\Phi_{\infty,geo} = 45°$, $\bar{R}_z = 5$–6 μm. I denotes the integral of the disturbance functions.

from the shape of an eigenfunction of linear theory. Considering only the maximum amplitude would no longer represent a comparable measure for the disturbance intensity. To overcome this problem, the amplitude functions of stationary and non-stationary modes were integrated in the wall-normal direction. This leads to the integral $I(q/Q_e) = 1/\delta \int_0^\delta q/Q_e \mathrm{d}z$ with the non-dimensional disturbance q/Q_e being either the amplitude of the stationary or the r.m.s. values of the travelling modes. In figure 14 the disturbance growth in the 1MK is shown without and with the additional screen for identical surface conditions. In comparison with figure 1(*b*) it becomes obvious that the strong saturation of the disturbance amplitudes prior to transition in figure 1 is partly due to the changes in the shape of the amplitude function that were not considered. Increasing the turbulence level from $Tu = 0.15\%$ (figure 14*a*) to 0.27% (figure 14*b*) results in the saturation amplitude of crossflow vortices being reduced considerably, while at the first measurement location $x_c/c = 0.4$ the crossflow vortices have similar amplitudes. Therefore the growth rate of the stationary modes at higher free-stream turbulence is clearly reduced. Also the non-stationary modes are less amplified in the higher-turbulence environment. However, the amplitudes at 40% chord are much higher than at the lower Tu, indicating the ability of free-stream turbulence to trigger travelling crossflow waves.

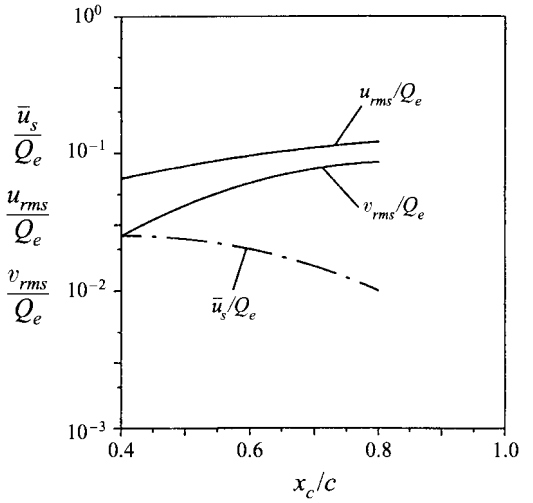

FIGURE 15. Spatial growth of stationary ($\bar{u}_s$) and non-stationary (u_{rms}, v_{rms}) instability modes in the NWG ($Tu = 0.57\%$) at $Q_{\infty,tun} = 19\ \mathrm{m\ s^{-1}}$, $\Phi_{\infty,geo} = 45°$, $\bar{R}_z = 5\,\mu\mathrm{m}$. $\bar{u}_s, u_{rms}, v_{rms}$ denote the local maxima of the disturbance functions.

A further increase of the turbulence level (NWG, $Tu = 0.57\%$) caused the disturbance growth displayed in figure 15. At the same chord Reynolds number as the previous experiments, stationary vortices now play a negligible role. Their amplitude even decreases with streamwise direction. The observed wavelength is approximately double that of the most unstable mode of linear theory. Non-stationary modes exhibit immense amplitudes of $u_{rms} \approx 7\%$ at the early measurement location of $x_c/c = 0.4$. Time history records showed intermittency along most of the measurement region, with a value of 50% at $x_c/c = 0.86$. Hence, in this wind tunnel by-pass effects may characterize the disturbance development.

Changes in Tu obviously affect not only the initial amplitudes of of travelling waves, but also the growth of both kinds of instability modes. The latter is in contrast to the results of local linear theory. The question arises of how to explain this effect of free-stream turbulence. Müller (1990) had found differences in the frequencies of the maximum amplitude of non-stationary modes in different test facilities. His data were supplemented in the present work by hot-film measurements in the water towing tank (WSG) and hot-wire measurements in the 1MK with the additional screen. As demonstrated in figure 16, there are mainly two frequency levels. In facilities with small free-stream turbulence ($Tu \leqslant 0.08\%$), only the higher frequency level of non-stationary instability modes at $2.8 < f^* = f x_c/Q_e < 3.6$ is observed. In this range the local linear stability calculations of Wagner (1992) showed the most amplified travelling waves. However, Fischer & Dallmann (1991) found strongly amplified secondary modes in a range of frequencies which is only slightly higher. These results prevent a clear interpretation of the observations. At higher free-stream turbulence travelling modes with maximum amplitudes are found in the range $1.3 < f^* < 2.5$, considerably lower than in low-turbulence environments. Although the measured amplitudes in the whole band of amplified frequencies $1.3 < f^* < 4.0$ do not exhibit very large differences (i.e. the power spectra reveal a rather flat maximum), the first question to be answered regards the reasons for this behaviour. Are there differences in the spectral distribution of turbulent fluctuations in various facilities which may lead to changes in the spectral content of the largest initial disturbance amplitudes?

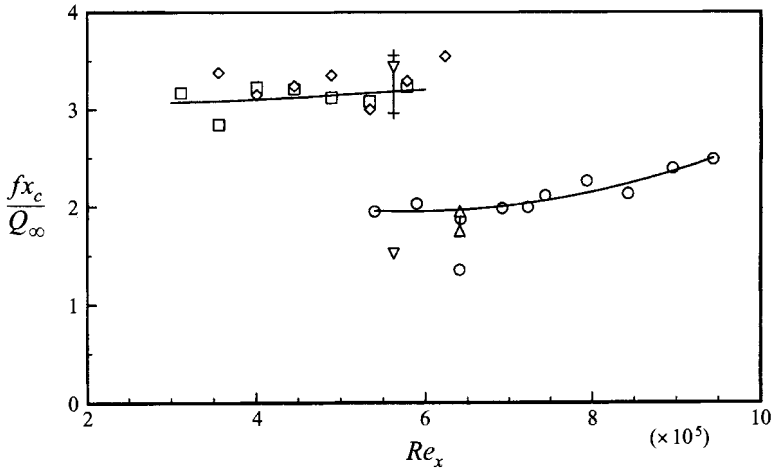

FIGURE 16. Dimensionless frequencies of maximum amplitude in the hot-wire power spectra measured in different test facilities at $x_c/c = 0.9$ and $z/\delta \approx 0.3$ in the unstable three-dimensional boundary layer. □, ◇, WSG, $\bar{R}_z < 1$ μm; ▽, NWB, $\bar{R}_z = 6$ μm; ○, 1MK, $\bar{R}_z = 5$–6 μm; △, 1MK plus screen, $\bar{R}_z = 6$ μm; +, spectrum of the most-amplified travelling modes calculated by local linear theory. In the 1MK and WSG the Reynolds number was varied with the free-stream velocity.

To answer this question, it was necessary to obtain some information on the spectral content of wind-tunnel turbulence. Because turbulence spectra were not available for the wind tunnels concerned, hot-wire measurements were performed. Using X-hot-wire probes the fluctuations in the test sections of the NWB, 1MK, 1MK plus screen, and NWG were measured. The method of determining turbulence levels by integrating the power spectra of velocity fluctuations permitted the quantitative comparison of spectra in different wind tunnels. A common feature of all the wind-tunnel configurations examined was the dominance of lateral fluctuations v', w' compared to the streamwise u'. Thus, the turbulence levels Tu should not be restricted to the streamwise fluctuations, but should consider the lateral components also, as done in the present study. In figure 17 the spectra of the streamwise velocity fluctuations are plotted for the four wind-tunnel configurations. On the abscissa the Strouhal number per unit length f/Q_∞ was used in order to account for differences in the free-stream velocity. The ordinate $(\Delta f G_u/Q_\infty^2)^{1/2}$ represents the dimensionless amplitude of each Fourier mode (with G_u being the power spectral density function and Δf the frequency resolution). The rather high turbulence level of the NWG ($Tu = 0.57\%$) may be due to flow separation in the curved diffuser of this facility. The long settling chamber, allowing a strong dissipation of small-scale eddies, is responsible for the steep decay of the spectrum above $f/Q_\infty = 20\ \mathrm{m}^{-1}$. In contrast to this, in the 1MK with the additional screen, i.e. with the shortest decay length, there are still relevant higher frequency fluctuations. In the frequency range of the most-amplified travelling waves $2.5 < f/Q_\infty < 8.5\ \mathrm{m}^{-1}$, however, the spectra of free-stream turbulence differ mainly in amplitude level: no distinct peaks were found. And indeed referring to figure 16 this seems to be of less importance for the level of frequencies with maximum amplitude: the additional screen does not show any considerable changes in this level. This simply suggests for the present experiments that the overall integrated turbulence level Tu is sufficient as a parameter to describe the influence of free-stream turbulence on the development of crossflow instabilities. Hence it can be stated that the width of the spectral content of free-stream turbulence seems to have no effect on the transition process and cannot explain the dependency on the disturbance development.

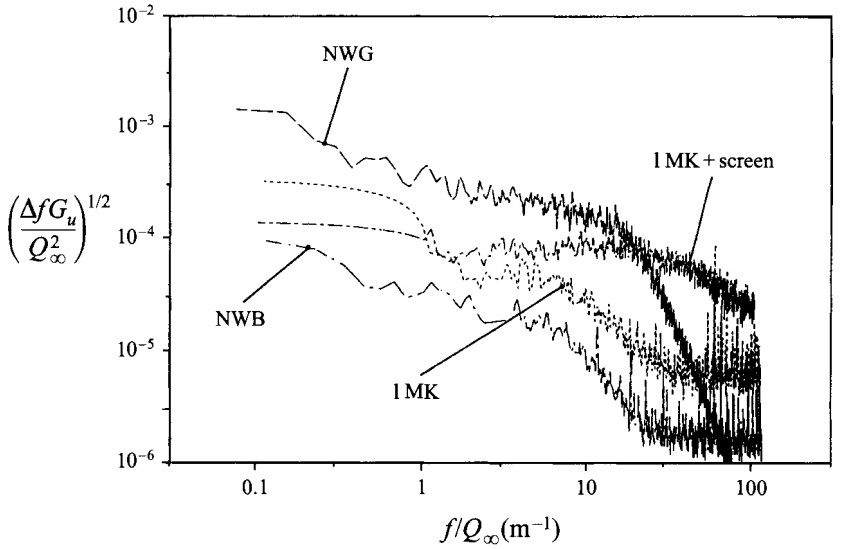

FIGURE 17. Spectral distribution of wind-tunnel turbulence (streamwise component u') in the different test facilities.

For the further study of possible reasons for this phenomenon, the r.m.s. values of travelling modes at the first measurement position $x_c/c = 0.4$ in the different facilities (figures 1, 14 and 15) are compared. It turns out that this level rises continuously with increasing free-stream turbulence. Not only the amplitude but also the growth rates of travelling modes differ considerably at this location. This indicates the very different amplitude level of travelling modes at the position of neutral stability. Hence, the three-dimensional boundary layer exhibits a strong receptivity to free-stream turbulence. A similar result is known from Blasius flow. In this two-dimensional base flow however, nonlinear effects characterize only a small part of the transition region and therefore the global changes in the disturbance growth seen in the three-dimensional boundary layer were not observed. One of the striking features of the latter, the dependence of the growth of stationary vortices on the development of the travelling waves, will be further discussed in the following sections where the effect of other disturbance sources is considered.

4.4.2. *Sound*

Another type of environmental disturbance that might be converted to non-stationary instability modes is sound waves. Experiments on the TS-instability in two-dimensional flat plate flows found sound waves of defined frequency and direction to be very efficient in promoting the transition process (see e.g. Leehey, Gedney & Her 1984; Kosorygin, Levchenko & Polyakov 1984). For TS-instabilities receptivity theories concerning long-wavelength acoustic disturbances have been developed (Goldstein & Hultgren 1989). In the case of crossflow instability Takagi *et al.* (1991) concluded from their experiments with artificial sound excitation in a wind tunnel that sound has no effect on the transition location on an infinite swept wing. Also no effect of acoustic disturbances was found by King (1992) on a conical model at incidence at high-speed flow, which was in contrast to the symmetric case. This is a surprising result, considering the strong effect sound has on the excitation of TS-instabilities found in the other studies above mentioned.

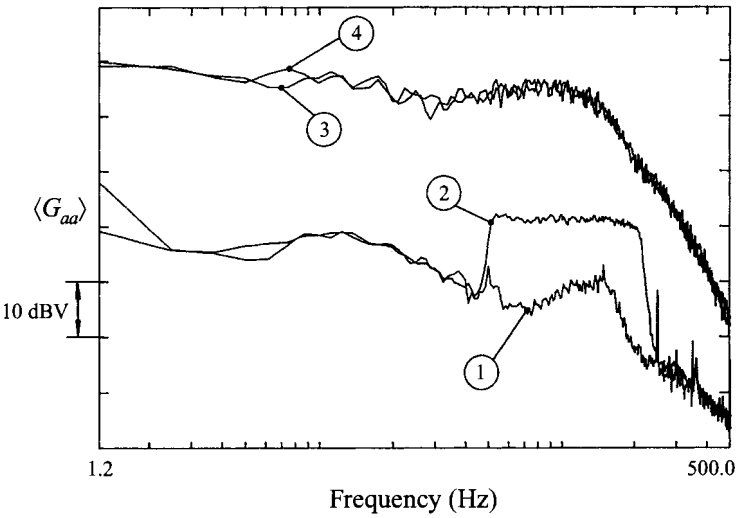

FIGURE 18. Spectra of hot-wire signals at two wall distances inside and outside the boundary layer at $x_c/c = 0.9$ with and without artificially excited sound ($Tu = 0.15\%$, $\bar{R}_z = 1.8$ μm, loudspeaker signal: band-pass filtered random noise $55 < f < 200$ Hz, SPL ≈ 103 dB). Outside the boundary layer at $z/\delta = 2.5$: curve 1 without sound, curve 2 with sound; inside the boundary layer at $z/\delta = 0.2$: curve 3 without sound, curve 4 with sound.

In the following this result was checked for the present experiment by artifically introducing sound waves in the 1MK with the set-up described in §3.1. A typical result of the effect on the instability development is presented in figure 18. The loudspeaker signal was chosen to be a band-pass-filtered random noise in the frequency range of amplified travelling instability waves with a considerable sound pressure level, SPL ≈ 103 dB. Outside the boundary layer (curves 1, 2) the effectiveness of the sound excitation is clearly visible in the excited frequency range. Inside the boundary layer (curves 3, 4) the amplitudes of travelling waves at this chord position are much higher than the amplitudes of the acoustic waves in the free stream (note the logarithmic scale in figure 18) and no difference was observed for the spectra of instability modes, neither in amplitude level nor in frequency range. Other experiments with pure sinusoidal excitation, sound pressure levels up to 111 dB and additional roughness elements on the flat plate close to the neutral position (which was shown e.g. by Saric 1992 or Bertolotti & Crouch 1992 to increase the receptivity to acoustic disturbances in the Blasius flow considerably) showed the same result. A final attempt was made by varying the position of the loudspeaker in order to change the propagation direction of the acoustic waves. However, positions below, behind and on the sides of the flat plate model exhibited no effect on the development of instabilities.

The results of these experiments suggest the conclusion that the velocity fluctuations in the free stream due to acoustic waves are merely superimposed on the disturbance flow field. No response of the disturbance amplitudes of the travelling modes to the introduced sound was observed at the measurement location. Additionally there was no change in the location of transition. These findings seem to confirm the surprising results of Takagi *et al.* (1991) and King (1992). Finally it should be noted that the present results were obtained for acoustic waves added to the ever-present acoustic field of the wind-tunnel flow. The effect of reductions of the latter could not be examined in this study.

4.4.3. *Non-uniformities of the test section mean flow*

It is known from experiments in Görtler flow that screens in wind tunnels produce small non-uniformities in the mean flow which initiate the longitudinal vortices. Correspondingly the wavelength of these Görtler vortices is given by these non-uniformities of the mean flow and does not depend on the stability parameter (Bippes 1972; Swearingen & Blackwelder 1986). The possibility that the stationary crossflow vortices, also a longitudinal vortex instability, are initiated or influenced by the screen flow field needed to be examined. In particular the qualitative agreement between the spanwise periodicity of $\bar{U}_s$ due to the crossflow vortices and the velocity distribution in the mean flow behind screens (visualized in a water towing tank and calculated by Böttcher & Wedemeyer 1989) seems to support this idea.

Therefore, an attempt was made to identify the screen-generated non-uniformities of the mean flow field in different wind tunnels and to check a possible relation with the development of crossflow vortices. The measurements for the detection of spatial mean flow variations of the order 10^{-3} to 10^{-4} Q_∞ are described in detail by Deyhle (1993). It was found that correlation measurements between a traversing and a fixed probe were required to separate the small spatial variations of the test section velocity from low-frequency temporal variations. Differences in the dominant wavelength of the test-section mean flow of different wind-tunnel configurations were clearly identified with this method and are presented in the above-cited reference. The experimental method adopted to identify a possible effect on the crossflow vortex wavelength was to vary the dominant wavelength of the spatial mean flow variations in the oncoming flow. This was done in the 1MK by introducing the additional screen, i.e. changing the distance between the last wind-tunnel screen and the model from $\Delta x = 4.1$ m to $\Delta x = 1.25$ m. Böttcher & Wedemeyer (1989) found this distance to be the only relevant geometry parameter for the dominant wavelength in the wake flow of screens. The dominant wavelength in the test section was reduced by the shorter distance (as expected qualitatively from the calculation) from 38 mm to 23 mm, which is still approximately twice the value of observed crossflow-vortex wavelengths. In figure 19(*a*, *b*) the results are plotted of two traversing measurements in the boundary layer on the same flat plate surface with and without the additional screen. In the case of initiation, the comparison of the crossflow vortex wavelengths of both measurements should exhibit a change, but no change can be detected. It turns out that even relative differences in the amplitudes of neighbouring vortices are preserved. The only difference observed is the uniform reduction of amplitudes. This can be seen more distinctly in the wavenumber spectra of the two spanwise distributions depicted in figure 19(*c*). The reduction of crossflow-vortex amplitudes is caused by the increased turbulence level (from $Tu = 0.15\%$ to 0.27%) and an associated decrease in the stationary vortex growth due to nonlinear disturbance interaction as shown before. A further comparison of the measured crossflow-vortex wavelength at earlier streamwise positions, $0.4 < x_c/c < 0.9$, showed the same results.

These observations imply that in the present experiment mean flow variations are not an effective means to initiate crossflow vortices as is the case for Görtler vortices. Thus the question arises of why there is a much stronger effect of screen-induced disturbances on Görtler vortices than on crossflow vortices. The answer may be that the flow on concave walls leads to an unstable stratification in the boundary layer in the wall-normal direction. Small displacements of fluid particles must initiate the Görtler vortices. This was demonstrated in the water towing tank experiments of Bippes (1972), where Görtler vortices could only be identified as a primary instability

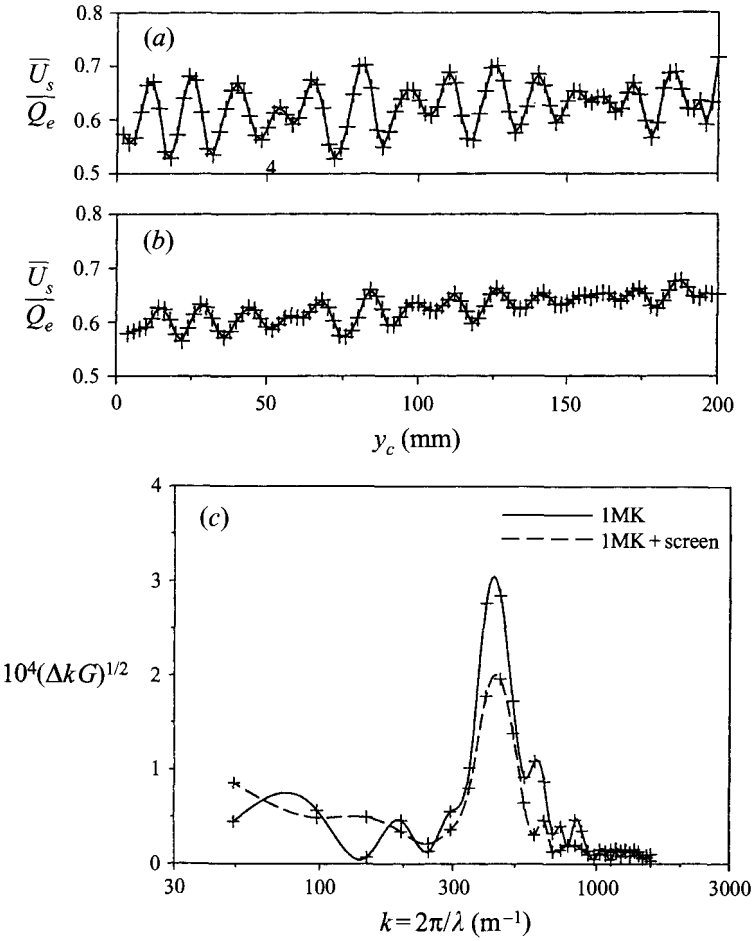

FIGURE 19. Spanwise periodicity of the mean velocity $\bar{U}_s$ in the three-dimensional boundary layer (*a*) without and (*b*) with the additional screen in the 1MK, measured at $x_c/c = 0.9$, $z/\delta \approx 0.25$, $Q_\infty = 19$ m s^{-1}, $\bar{R}_z = 1.8$ μm. (*c*) Wavenumber spectra were calculated from both spanwise variations (*a*) and (*b*).

when a screen was towed in front of the model. In this case both kinds of screen-induced disturbances, i.e. turbulence and non-uniformities of the mean flow, promote the development of Görtler vortices. Without the screen the transition process showed the same features as in Blasius flow. In contrast, in the present water towing tank tests on crossflow instability, stationary vortices developed as dominating instability mode without a screen, even on a very smooth surface with an overall roughness of $\bar{R}_z <$ 1 μm. In the flow visualizations non-stationary instability modes could only be detected immediately before the final breakdown of laminar flow. These results imply that in the presence of crossflow instability there must exist another mechanism for the stimulation of stationary vortices. The essential effect of screen-generated disturbances is the stimulation of travelling crossflow modes via turbulent fluctuations.

4.4.4. *Surface roughness*

Another possible reason for the strong spatial reproducibility of the crossflow-vortex pattern in subsequent test runs might be the excitation of crossflow vortices by surface roughness. To check this, the swept flat plate was shifted in the spanwise direction by

Müller & Bippes (1988) and Deyhle (1993). It turned out that the vortex pattern of the disturbed boundary-layer flow, i.e. the spanwise variation of wavelength and amplitude of individual crossflow vortices, was shifted with the model. On the one hand this result confirmed the lower-order effect of screen-induced mean flow distortion on the wavelength selection of crossflow vortices. On the other hand it indicated the surface roughness to be a more effective source for the stimulation of crossflow vortices. Further evidence for that was established by Müller & Bippes (1988) and Müller (1990). After having increased the surface roughness, they observed an earlier saturation of the stationary instability mode at a level 50% higher than the result obtained on the smoother surface. At the same time Saric (1989, personal communication) found that polishing the surface of a swept wing at locations of strong streamwise vortex development leads to a reduction of the vortex amplitudes and to a delay of transition. These observations suggest that surface roughness is the main source of stationary vortex formation and so should be studied in detail in order to improve the understanding of the transition processes in three-dimensional boundary layers. Further experiments of Saric and co-workers (Radeztsky *et al.* 1993; Radeztsky, Reibert & Saric 1994) showed that tiny discrete roughnesses can initialize the crossflow vortices. Their experiments were focused on the effects of surface roughness on the transition location, and the influence on initialization, wavelength selection, nonlinear development and growth of streamwise vortices was not considered. But knowledge of those physical aspects is a necessary basis for a well-founded transition prediction, i.e. for comparison with PSE and DNS analyses. Therefore the present study throws some additional light on these aspects of the roughness problem. In particular, attempts were made to answer questions of practical relevance, such as the dependence of receptivity of the three-dimensional boundary layer to roughnesses of different shape, size, location and distribution.

Early experiments with an overall roughness of the flat plate of $\bar{R}_z \approx 6$ μm ($\bar{R}_z$ represents an average peak-to-peak roughness value) showed that wiping the surface with a soft cloth changes the vortex pattern considerably. Therefore, the first studies were aimed at finding a roughness level which allows reproducible measurements. Such conditions could be found by successive sanding and polishing to a level of $\bar{R}_z =$ 1.8 μm and by careful cleaning of the attachment line region even of dust particles. For this roughness condition the disturbance growth was traced and compared with the data of Müller (1990) taken on a sanded surface ($\bar{R}_z = 6$ μm) and with sandpaper glued on the flat plate surface ($\bar{R}_z = 40$ μm). The growth of stationary and travelling modes on the three different surface qualities, measured in the same 1MK wind-tunnel configuration at $Tu = 0.15\%$, is presented in figure 20. Comparing the amplitudes at $x_c/c = 0.4$ it turns out that the amplitudes of the crossflow vortices at this location increase with increasing surface roughness. The observed growth curves of the vortices for the two lower roughness levels seem to be only shifted in amplitude with nearly the same growth rate in the region of linear growth. Hence the saturation level is reduced by a factor of 2 from 9% at the moderate roughness to 4.5% at the polished surface. Furthermore, the roughest surface causes the growth of stationary vortices to be saturated much earlier, namely at $x_c/c \approx 0.75$, reaching the highest amplitudes of 14.5%. The corresponding growth of the travelling modes for the two lower roughness levels is not affected by the different amplitude levels. However, in the case of high roughness and high saturation levels the travelling modes exhibit the same behaviour of very early splitting of the growth along streamwise zones of minimum and maximum mean velocity $\bar{U}_s$ as in the case of low turbulence (compare figure 1*b*) or artificial stimulation of the stationary modes (compare figure 23). Stronger stimulation leads to

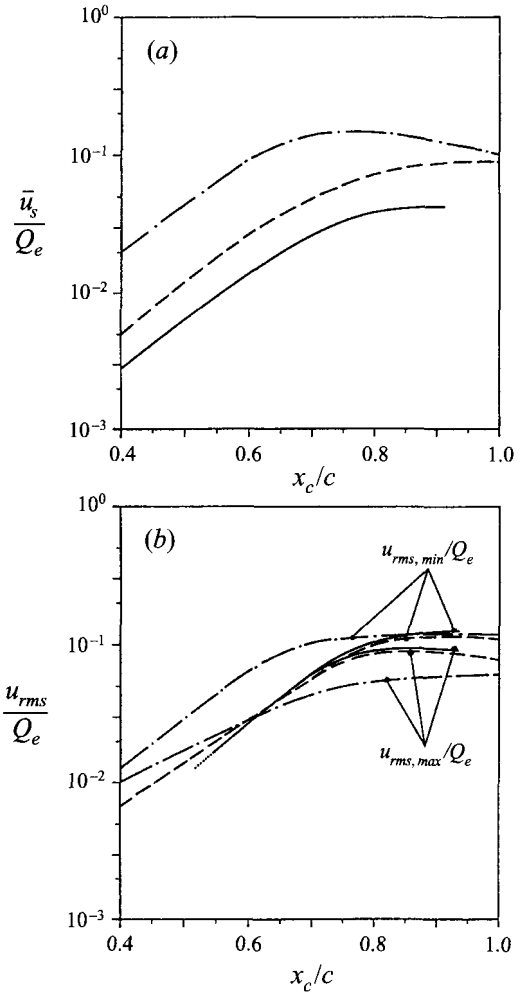

FIGURE 20. Spatial growth of (*a*) stationary ($\bar{u}_s$) and (*b*) non-stationary (u_{rms}) instability modes on different flat plate surface qualities in the 1MK. $\bar{u}_s$ and u_{rms} denote the local maxima of the disturbance functions. ·····, sandpaper $\bar{R}_z = 40$ μm; – – –, wooden plate $\bar{R}_z = 6$ μm; ——, polished aluminium plate $\bar{R}_z = 1.8$ μm.

earlier saturation of the stationary crossflow vortices at higher amplitudes. As a result it was found that roughness stimulates the crossflow vortices but not the travelling modes in the roughness range studied. The growth of the unsteady modes on these three roughness levels at constant free-stream turbulence seems to be only affected by secondary effects. No change of the crossflow vortex wavelength was observed. At all roughness levels approximately the value of the most amplified vortex wavelength was selected.

For a detailed study of the initiation of instabilities by surface roughness, discrete artificial roughness elements on the swept plate surface were used. Of special interest was the question of whether the flow around these elements influences the wavelength selection and whether defined wavelengths of the stationary vortices can be stimulated. Therefore roughness elements (see § 3.1) of different shape, size and height were applied at different downstream locations on the polished surface ($\bar{R}_z = 1.8$ μm) of the swept flat plate. The effect of a two-dimensional shape of a roughness element, i.e. a strip of

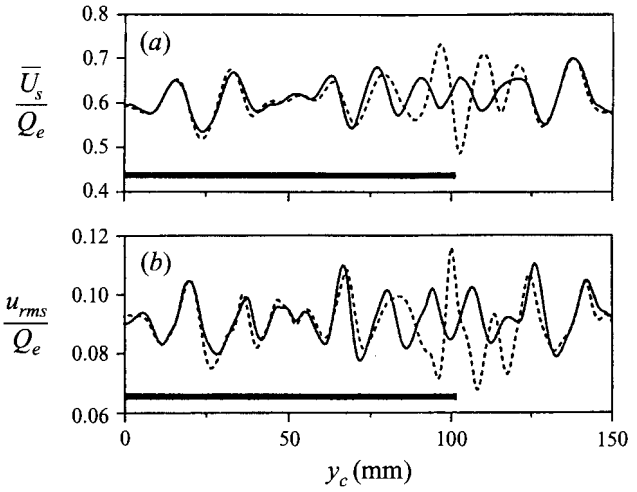

FIGURE 21. Spanwise distribution of (*a*) $\bar{U}_s$ and (*b*) u_{rms} in the boundary layer at $x_c/c = 0.9$ without (——) and with (· · · · · ·) an artificial two-dimensional roughness strip measured in the 1MK. The region influenced by the strip can be given only approximately, because the measurement was performed far downstream of the roughness location.

uniform height in the spanwise direction y_c, was considered first. This strip of 160 mm length ($\approx$ 14 vortex wavelengths), 1.5 mm width and 10 μm height ($h^+ \approx 0.45$, see §3.1) was attached parallel to the leading edge at 5.6% chord. In figure 21(*a*, *b*) its influence on the spanwise velocity distribution $\bar{U}_s(y_c)$ and the r.m.s. distribution $u_{rms}(y_c)$ is compared with that on the smooth surface. Only the region $70 < y_c < 125$ mm was found to be strongly affected by the strip: there the spanwise formation of the vortices is changed and the stationary vortex amplitudes are increased by a factor of 3. This spanwise region corresponds to the three-dimensional end of the strip. Surprisingly, the disturbance flow downstream of the two-dimensional part of the strip showed no difference to the smooth wall. This is in contrast to effects of such a roughness step in the two-dimensional Blasius flow. In this viscous instability the short time adjustment of the flow behind a step causes global changes in the stability characteristics. In the dynamically unstable three-dimensional boundary layer neither initialization nor growth of stationary and travelling disturbance modes are affected by two-dimensional roughness. It is suggested that only roughness-generated longitudinal vorticity is the important factor. Spanwise vorticity, at least with the heights used in the present work, has no effect on the disturbance development. Therefore it is sufficient to examine the role of three-dimensional roughness elements with heights of $h^+ = O(1)$.

Of further interest are the streamwise location and the height of maximum receptivity to such discrete roughness elements. The application of roughness elements of identical physical height at different streamwise positions, i.e. at different thicknesses of the local boundary layer, raises the question of whether the effects can be compared directly. The important parameter to characterize roughness effects is considered to be the height in non-dimensional wall units $h^+ = u_\tau h/\nu$, because it represents a measure of the vorticity in the wall region for the limit of vanishing roughness height $h \to 0$. From boundary-layer calculations it could be shown that even in the leading-edge region the friction velocity $u_\tau = (\tau_w/\rho)^{1/2}$ is approximately constant with x_c and so are the values of h^+. Therefore the effects of the same roughness height at different downstream locations can be compared directly with each other. The three-dimensional roughness elements used in the following experiments are circular dots with different

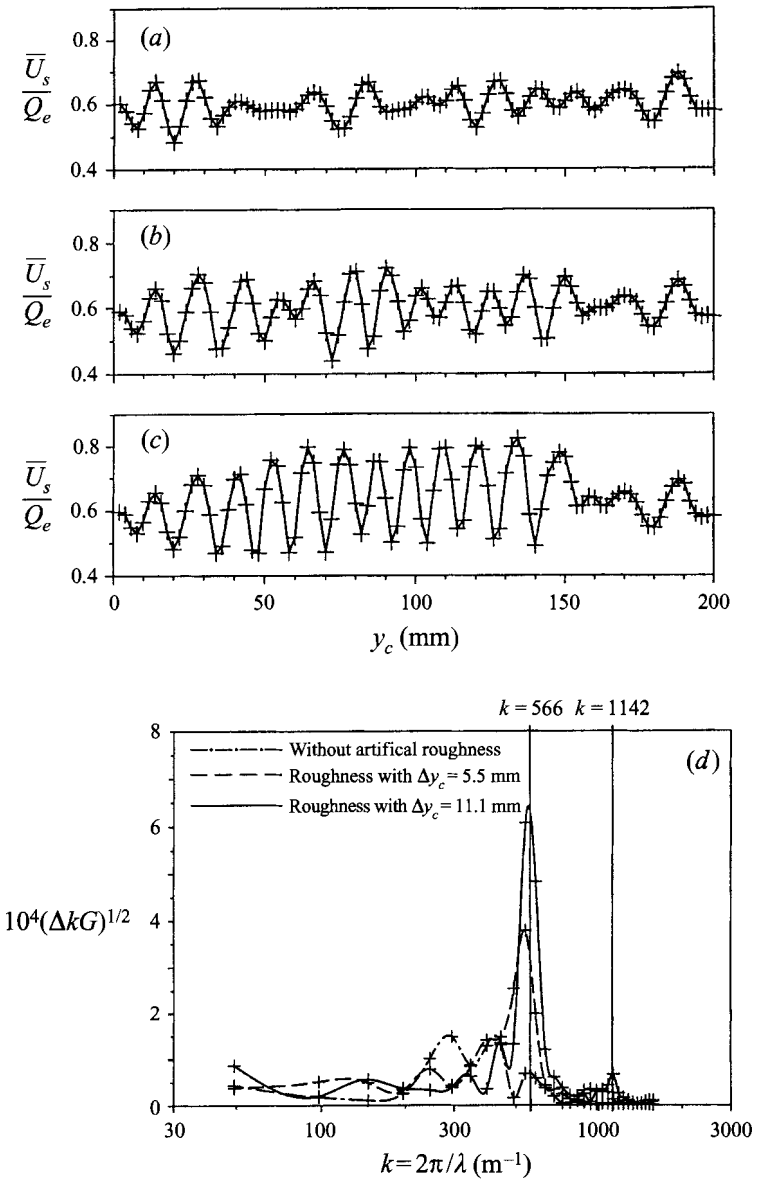

FIGURE 22. Spanwise velocity distribution $\bar{U}_s(y_c)$ in the boundary layer at $x_c/c = 0.9$, $z/\delta \approx 0.25$ (*a*) without and with artificial roughness dots of different spanwise spacing (*b*) $\Delta y_c = 5.5$ mm and (*c*) $\Delta y_c = 11.1$ mm measured in the 1MK. In (*d*) the wavenumber spectra of (*a*) and (*b*) are represented.

diameters d_h. They were applied with different spanwise spacings Δy_c at a constant x_c-position.

Experiments with a single roughness dot of diameter $d_h = 3.2$ mm and increasing height $h = 10$, 20 and 30 μm showed that the increase in crossflow-vortex amplitudes at a x_c-location of 90% chord is the same for $h = 10$ μm as for 20 and 30 μm, but more of the neighbouring vortices are affected, i.e. the region of influence in the spanwise direction increases. Hence, the following experiments were performed using only a roughness height of 10 μm. In order to find the streamwise position of maximum receptivity of the boundary layer to the discrete roughness elements, the same pattern

of dots was applied at different downstream locations $0.021 \leqslant x_c/c \leqslant 0.16$. This range covers the position of neutral stability of the most-amplified stationary vortex mode at $x_c/c = 0.08$ as calculated by Wagner (1992). Measurements at $x_c/c = 0.9$ indicated the strongest effects for a roughness location around 8% chord, i.e. around the neutral stability boundary (Deyhle 1993). The same roughness closer to the attachment line caused lower amplitudes of the crossflow vortices at the measurement position although the ratio of roughness height to boundary-layer thickness is much larger in this region. Further experiments with different diameters of the dots at constant spanwise spacing Δy_c showed maximum vortex amplitudes for a diameter of $d_n \approx 0.3\Delta y_c$. In this case the regions of longitudinal vorticity with alternating direction of rotation behind the roughness elements might be equally spaced and can trigger the crossflow-vortex pattern best.

The same result was found by varying the spanwise spacing Δy_c but keeping the diameter of the roughness dots constant. In figure 22 the velocity distributions at two spanwise spacings, $\Delta y_c = 5.5$ mm and $\Delta y_c = 11.1$ mm, the latter being very close to the most-amplified vortex wavelength, are compared with the smooth surface. The region $30 < y_c < 150$ mm is influenced by the roughness dots. A much more regular vortex pattern is observed in the case of the spacing close to the naturally selected vortex wavelength, in contrast to the lower value. The amplitudes of the modes can be easily compared by considering the wavenumber spectra of the three distributions in figures 22(*a–c*), given in figure 22(*d*). The vortex wavelength with the largest amplitudes for both roughness cases is very close to the naturally selected one, although the stimulated wavenumbers differ by a factor of 2 (wavenumber $k = 2\pi/\lambda = 566\ \mathrm{m}^{-1}$ corresponds to $\Delta y_c = 11.1$ mm, $k = 1142\ \mathrm{m}^{-1}$ to $\Delta y_c = 5.5$ mm). The amplitude found for the stimulation with $\Delta y_c = 11.1$ mm is approximately 1.7 times higher than with the smaller dot spacing.

The ability of discrete roughness elements to initialize a very regular crossflow-vortex flow field allows their use as a disturbance generator. This offers the opportunity to study the disturbance development dominated by strong crossflow vortices under otherwise the same flow conditions as in earlier experiments. Circular roughness elements were applied in the spanwise distance that initialized the naturally selected crossflow-vortex wavelength best. The growth of instability modes obtained in the 1MK at $Tu = 0.15\%$ is presented in figure 23. Compared with the NWB experiment at $Tu = 0.08\%$ and $\bar{R}_z = 6$ μm, similarly high saturation amplitudes of crossflow vortices and the associated splitting of the growth of r.m.s. values of travelling modes along streamwise zones of minimum and maximum mean velocity $\bar{U}_s$ were found. The roughness elements cause the splitting to be more pronounced, with even a decrease of amplitudes $u_{rms,max}$ in the region $0.7 < x_c/c < 0.8$. The main advantage of this experiment is the very regular disturbance flow field and the known initial roughness conditions. Therefore it can serve as reference data for the comparison with PSE (as was done by Bertolotti & Bippes 1994; Bertolotti 1994) and DNS stability analyses.

All these experiments indicate that roughness is responsible for the formation of longitudinal vortices in the three-dimensional boundary layer. Roughness heights h^+ of order one are sufficient to enhance the initialization of crossflow vortices, as long as longitudinal vorticity is introduced into the boundary layer. The strongest receptivity of the unstable boundary layer was found in the region of neutral stability for a spacing of roughness elements equivalent to the most unstable vortex wavelength and a diameter of $d_h \approx 0.3\Delta y_c$. Two-dimensional roughness with a similar height affects neither stationary nor travelling disturbances. Owing to nonlinear effects not only is the stimulation of crossflow vortices dramatically enhanced by roughness, but their

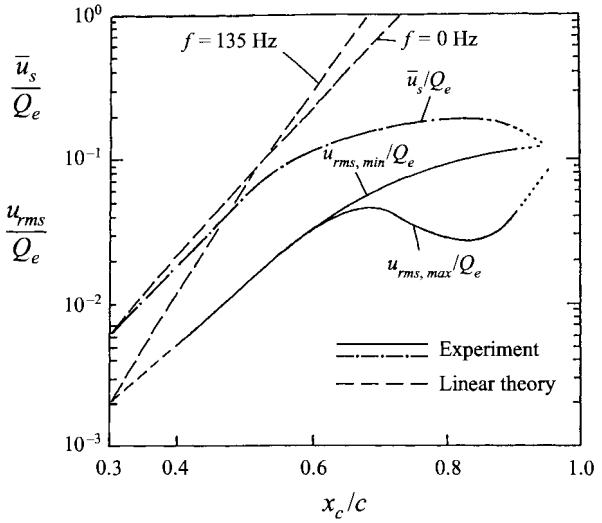

FIGURE 23. Spatial growth of stationary ($\bar{u}_s$) and non-stationary (u_{rms}) instability modes in the 1MK using discrete roughness elements ($d_h = 3.3$ mm, $h = 10$ μm, $\Delta y_c = 11.1$ mm at $x_c/c = 0.08$) on the polished plate surface ($\bar{R}_z = 1.8$ μm) to stimulate artificially crossflow vortices. $\bar{u}_s, u_{rms}$ denote the local maxima of the disturbance functions.

growth and saturation amplitude are also influenced. Together with free-stream turbulence, which initializes the travelling instability modes, roughness determines the amplitude ratio of stationary and travelling modes and therefore the path to transition. Among the four environmental conditions considered in the present experiments, free-stream turbulence and surface roughness are higher-order effects than sound and non-uniformities of the test section mean flow. Hence, the relevant parameters for describing the crossflow transition process are Tu and h^+.

4.5. *Transition*

As shown in figures 1, 14 and 20, under all environmental conditions investigated, the steady as well as unsteady disturbances grow until they arrive at a certain saturation level. This level depends on the initial conditions as described in the last section. Transition occurs some distance downstream. Hence, for the prediction of transition a major question is what event leads to transition after the disturbances have arrived at the saturation level. In flow visualizations performed in a water towing tank, i.e. in a disturbance environment similar to free flight conditions, unsteady modes can only be identified in the stationary vortex field at the very end of the transition process. But then they undergo an almost explosive growth which immediately leads to transition. In the visualization this looks like a bursting of individual stationary vortices. Measurement in the 1MK ($Tu = 0.15\%$) under controlled excitation of the stationary instability mode showed the appearance of high-frequency disturbances prior to the local breakdown of laminar flow (figure 24*a*, *c*). In the instantaneous signal this high-frequency mode manifests itself as high-frequency riders on the existing waves (see the small-amplitude high-frequency distortion in the time history record at $36 < t < 40$ ms in figure 24*a*). That means the amplitudes are very small and it may appear doubtful whether this phenomenon can initiate the sudden breakdown observed in flow visualizations. A quite similar phenomenon, however, was observed by Poll (1985) and in more detail by Kohama *et al.* (1991). The latter measured considerably larger amplitudes. One reason may be that this unsteady event occurs at arbitrary locations

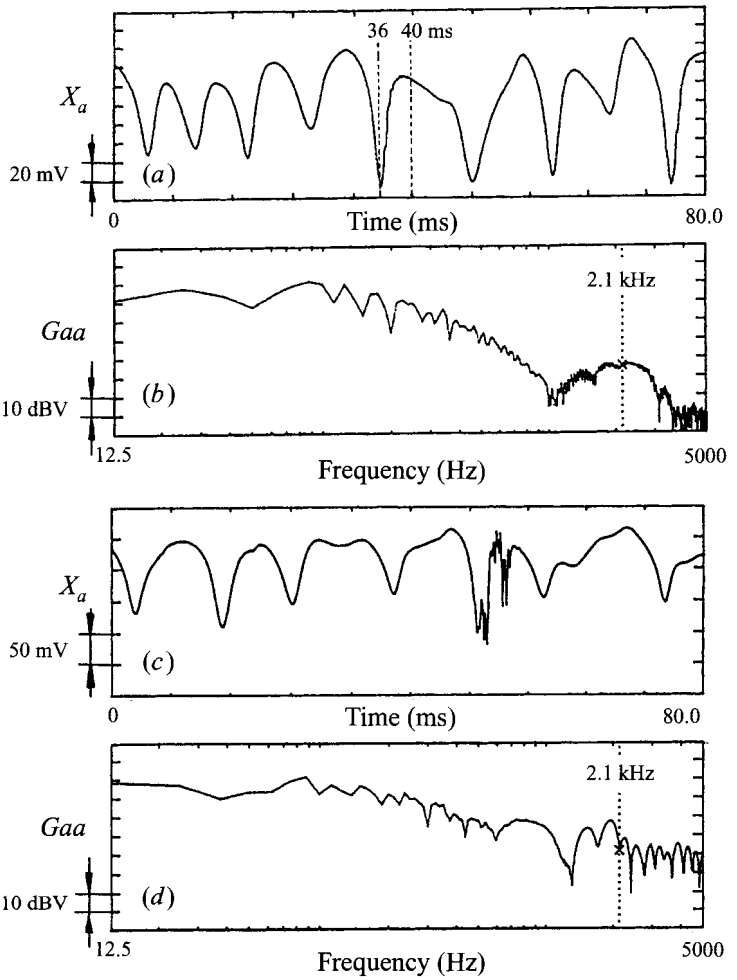

FIGURE 24. Secondary instability preceding the final breakdown: (*a*, *c*) two instantaneous hot-wire signals and (*b*, *d*) the corresponding power spectra, obtained under the same conditions in the 1MK ($Tu = 0.15\%$) on the polished aluminium plate ($\bar{R}_z = 1.8$ μm).

in the spot range. Measurements at fixed locations do not necessarily capture the most developed state while passing the hot-wire. Another reason may be that these high-frequency disturbances originate and are centred at locations of high shear generated in the stationary vortex field (in figure 8*c*, *d* those regions of high shear are indicated by small distances between isolines). Unfortunately, the measurements in the present study were not focused on those regions. Furthermore, in a lower-turbulence environment where the streamwise vortices end up at higher amplitudes and where the regions of high shear become more distinct, the formation of the wave riders can be traced more easily. It should be mentioned that for Blasius flow Koch (1992) found a resonance of secondary instability modes resulting in an algebraic amplification at Reynolds numbers where transition is observed. Although such a phenomenon could not yet be established in the case of three-dimensional boundary-layer flows it could explain the sudden breakdown observed in the visualizations. Currently no well-established theory is known which explains the experimental observations and the conditions for their appearance.

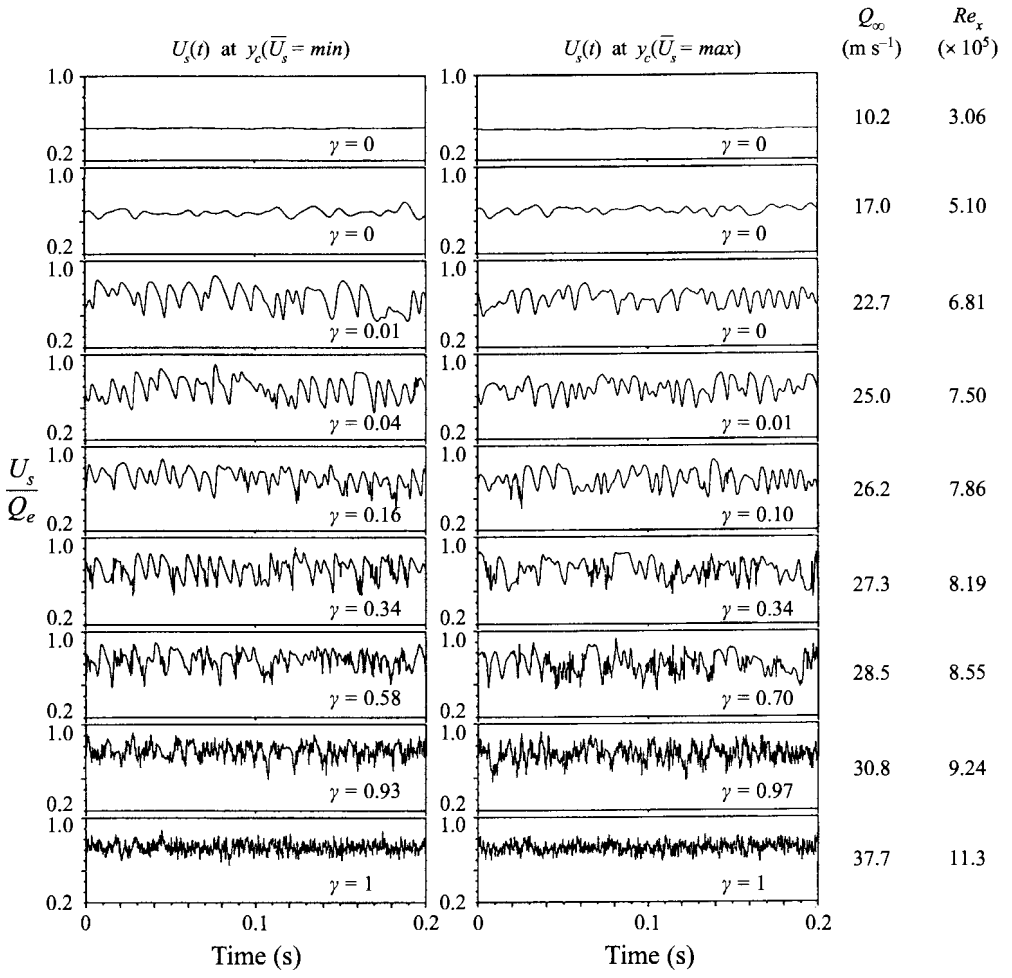

FIGURE 25. Time signals $U_s(t)$ at $x_c/c = 0.9$, $z = 0.75$ mm in the three-dimensional boundary layer at spanwise positions of minimum and maximum mean velocity during transition ($Tu = 0.15\%$, $\bar{R}_z = 1.8$ μm).

Of special practical interest is the dependence of the final onset of turbulent flow, i.e. the transition Reynolds number $Re_{x,tr}$, upon the initial conditions. According to the results of §4.4, only free-stream turbulence and three-dimensional surface roughness have to be considered as relevant environmental disturbance characteristics. In order to find hints for how to correlate the disturbance environment with transition location, transition was traced at the various environments described above.

Among different approaches to define a transition Reynolds number $Re_{x,tr}$, the most appropriate criterion of transition has to be chosen for the actual flow. In the continuous transition process from laminar to turbulent state this requires the selection of a well-defined location which allows quantitative comparisons. The gradual change of the shape factor H_{12} or the minimum of the wall shear stress do not meet the requirements. A better identification of the boundary-layer state during transition is given by the time records. The signals of a hot-wire probe located at a fixed position in the boundary layer are presented for different free-stream velocities in figure 25. The variation of Q_∞ causes the transition region to be shifted over the probe location. The data were acquired at two spanwise positions, identified at $Q_{\infty,tun} = 19$ m s^{-1}, of

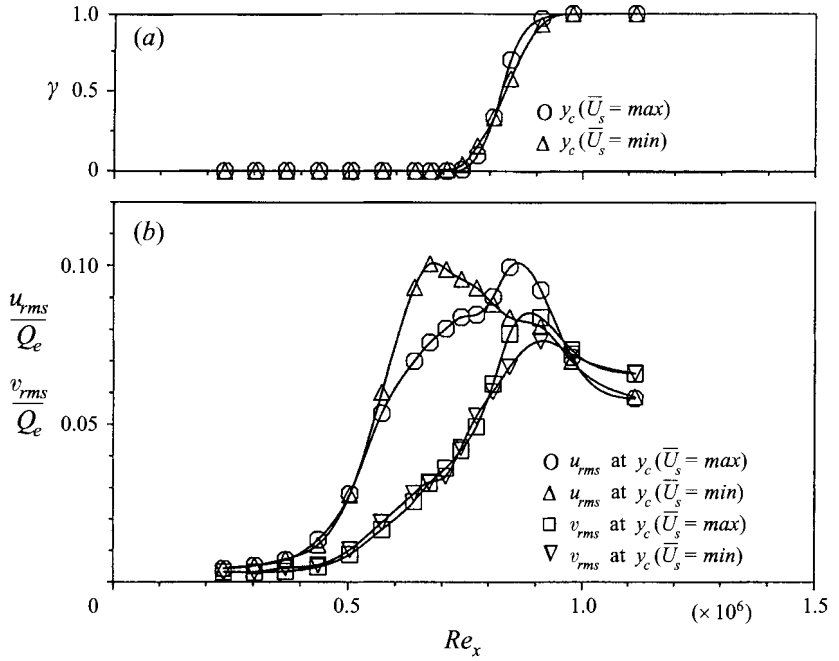

FIGURE 26. (*a*) Intermittency function γ and (*b*) r.m.s. values u_{rms}, v_{rms} at spanwise positions of minimum and maximum mean velocity during transition at $Tu = 0.15\%$ on the polished plate surface ($\bar{R}_z = 1.8$ μm), measured at $x_c/c = 0.9$, $z = 0.75$ mm.

minimum and maximum mean velocity $\bar{U}_s$ for $Tu = 0.15\%$ and a surface roughness of $\bar{R}_z = 1.8$ μm. With the probe position at constant $x_c/c = 0.9$ and the effective free-stream velocities the Reynolds numbers Re_x were calculated. As can be seen in figure 25, at $Re_x > 5 \times 10^5$ travelling crossflow waves with a rather regular periodicity are clearly visible. When $Re_x = 7.5 \times 10^5$ is reached, for the first time some high-frequency events were found at a location of minimum mean velocity. At a maximum of $\bar{U}_s$ this is observed first at a higher $Re_x = 7.9 \times 10^5$. With increasing Reynolds number the high-frequency portion of the signal increases. At $Re_x = 1.1 \times 10^6$ a fully turbulent state is reached. The clear distinction of high- and low-frequency portions of the signal suggests the determination of the intermittency function γ, defined as the time fraction of turbulent flow. The values obtained are also given in figure 25. For all the measured Reynolds numbers γ is plotted in figure 26 together with the r.m.s. values. The increase of $\gamma(Re_x)$ in the transition region appears steep and differences in maximum and minimum mean velocity are small around $\gamma = 0.5$. Therefore, the value of 50% intermittency was chosen as a clearly defined location in the transition process. This method provides a much better criterion than the maximum of r.m.s. values which spreads for u_{rms} and v_{rms} in the two measurement positions between $6.8 \times 10^5 < Re_x < 9.2 \times 10^5$ (compare figure 26*b*). The transition process at these specific environmental conditions is characterized by strong travelling modes reaching higher amplitudes than the crossflow vortices, which have already saturated at $A_s = 4.5\%$.

In the case of artificially increased roughness using dots in the region of neutral stability, the intermittency function and r.m.s. values are given in figure 27. The transition Reynolds number $Re_x = 7.1 \times 10^5$ at $\gamma = 0.5$ was found to be 14% lower than on the smooth surface. Now the crossflow vortices dominate the transition process, saturating at a higher level of $A_s = 15\%$. The r.m.s. values reach their

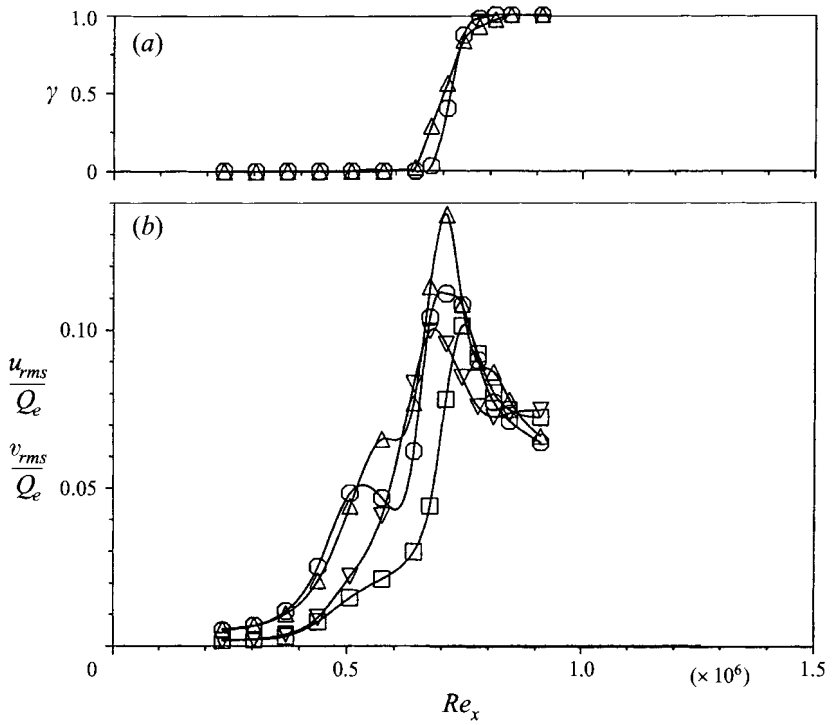

FIGURE 27. As figure 26 but with artificial roughness elements (d_h = 3.3 mm, h = 10 μm, Δy_c = 11.1 mm at x_c/c = 0.08).

maximum at almost the same Reynolds number where the intermittency function is equivalent to 50%. The maximum amplitude of u_{rms} at $\bar{U}_s$ = min was found to be higher (13.5%) than on the smooth surface (10%).

The intermittency function and transition Reynolds number were determined for all the wind tunnels and surface roughness conditions under consideration. The data are presented in table 1. The comparison of transition locations at a constant turbulence level of Tu = 0.15% in the 1MK exhibits a variation of more than 20% of $Re_{x,tr}$ due to different surface roughness. More surprisingly, however, is the fact that at the lower turbulence level in the NWB the transition location on the same surface quality is shifted upstream. In order to find a possible correlation of $Re_{x,tr}$ with turbulence level Tu and surface roughness h^+ the Reynolds numbers were plotted as a function of saturation amplitude A_s of the crossflow vortices in figure 28. All the points in this figure seem to be located on a unique curve. This result indicates that the growth and especially the saturation amplitude of the crossflow vortices determines the transition location. The distinct maximum of this curve is found at saturation amplitudes of A_s = 4–5%. In this case stationary and travelling modes show a comparable growth. The most delayed transition location therefore is found not for the lowest turbulence level but for environmental conditions which provoke a limited growth of the stationary vortices. Owing to nonlinear effects this is achieved by a corresponding growth of travelling modes initiated by a moderate turbulence level. Lowering the turbulence level, i.e. following the curve in figure 28 to the right, causes a dominance of the stationary vortices. Their higher saturation level of crossflow vortices leads to strongly amplified secondary instabilities, indicated in figures 1(*b*) and 23 by the splitting in the growth of the r.m.s. amplitudes. This lowers the transition Reynolds number. Increasing the

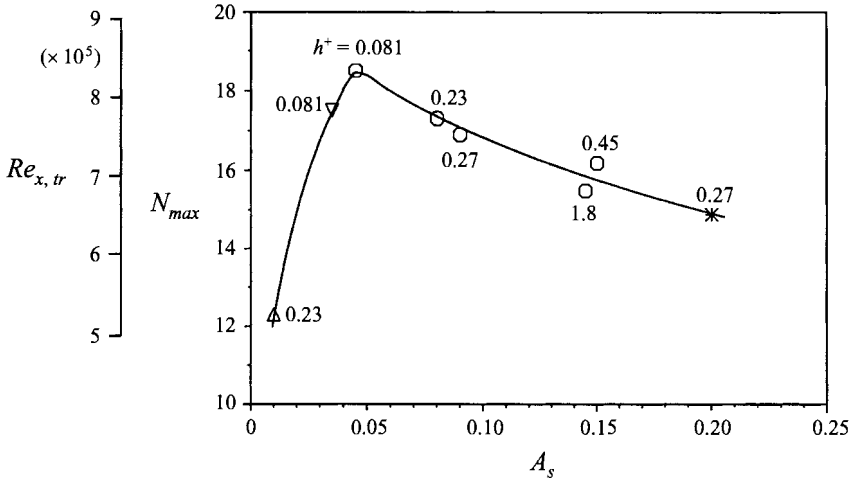

FIGURE 28. Dependence of transition Reynolds number and N-factor on the saturation amplitude A_s of stationary crossflow vortices for different turbulence levels and surface conditions. ✳, NWB, $Tu = 0.08\%$; ○, 1MK, $Tu = 0.15\%$; ▽, 1MK plus screen, $Tu = 0.27\%$; △, NWG, $Tu = 0.57\%$.

turbulence level, i.e. following the curve to the left, means strong primary amplification of travelling modes which lowers $Re_{x,tr}$ also. The important result for transition prediction is that in a low-turbulence environment, as under free flight conditions, the location of transition is essentially determined by surface roughness.

5. Conclusions

The governing instability feature, leading to transition of three-dimensional boundary layers subject only to crossflow instability, is the formation of streamwise vortices as the primary instability. They cause a distortion of the base flow and make the boundary layer susceptible to secondary instabilities. The consequence is a nonlinear development which is observed to start as soon as the amplitudes of the streamwise vortices become of measurable size. This extended range of nonlinear development covers the complete transition region accessible to clearly reproducible measurements.

For this reason it is very difficult to study the linear range of amplification under natural conditions of transition. An attempt has been made to artificially stimulate the instabilities at crossflow Reynolds numbers as close as possible to the critical value. However, to date it has only been possible to initiate the stationary vortices. As in the tests under natural conditions of transition the instabilities first identified correspond to those predicted by local linear linear theory. And in agreement to that, the travelling modes are now more amplified than the stationary modes. However, the growth of both kinds of modes is considerably weaker than predicted by linear theory. Spanwise-periodic amplitude variation of the unsteady modes having the same wavelength as the stationary vortices suggest that this is due to a nonlinear development caused by the distortion of the base flow by the stationary vortices. This became more obvious in the tests performed under natural conditions of transition. In order to obtain instabilities of measurable size for these tests, a larger Reynolds number had to be chosen. Under those conditions the observed downstream development revealed features predicted by nonlinear theories as due to nonlinear interactions: the deformation of the spanwise-averaged mean flow; the downstream attenuation of the growth of the disturbances until they end up at saturation; and the spanwise modulation of the amplitudes of the

travelling modes connected with a splitting in their growth measured along streamwise zones of maximum and minimum mean flow which are caused by the stationary vortices.

The most characteristic and striking features of the transition process under the action of crossflow instability are the early nonlinear disturbance development and the dependence on the upstream conditions. Tests performed on the same model in systematically varied disturbance environments revealed that in the presence of crossflow instability the boundary layer is most sensitive to surface roughness. The larger the roughness height, the larger the saturation level and the earlier transition occurs. In contrast to two-dimensional boundary layers, up to moderate values free-stream turbulence affects transition only indirectly. It attenuates the growth of the stationary vortices and retards transition. Only at values $Tu > 0.2\,\%$, depending on the roughness height, do travelling modes become dominating. A further increase of free-stream turbulence then accelerates transition. The receptivity to a two-dimensional surface protuberance and especially sound was observed to be very weak. Theoretical approaches applied to the present experiment showed that the transition process in the presence of crossflow instability can only be described using non-local nonlinear theories. The most urgent problem is the correct modelling of the initial conditions as regards surface roughness and free-stream turbulence. Comparison of the results obtained in the case of artificial initiation of the stationary instability mode with a nonlinear PSE analysis indicated that the saturation level can be predicted. From the present investigations it is this saturation level of crossflow vortices that determines the location of transition.

Since transition occurs at some downstream distance after the stationary vortices have saturated, for the direct prediction of transition the event which starts the almost explosive final breakdown observed in the experiment has yet to be described. For Blasius flow a resonance of secondary instabilities leading to an algebraic disturbance growth has been identified theoretically at Reynolds numbers where transition is observed in the experiment. If such an event could also be found in the case of crossflow instability, then the problem of transition prediction would be reduced to the solution of the receptivity to surface roughness and free-stream turbulence.

The authors wish to express thanks to Fabio Bertolotti for calculating the boundary-layer flow and the non-local stability analysis of the present experiment. The contributions of all colleagues inspiring this work with discussions are greatly acknowledged.

REFERENCES

ARNAL, D., COUSTOLS, E. & JUILLEN, J. C. 1984 Experimental and theoretical study of transition phenomena on an infinite swept wing. *Rech. Aerosp. No.* 1984-4.

BERTOLOTTI, F. P. 1994 A partial simulation of receptivity and transition in 3-D boundary layers. *IUTAM Symposium on Laminar-Turbulent Transition, Sendai (Japan), Sept. 5–9.*

BERTOLOTTI, F. P. & BIPPES, H. 1994 An experimental and computational investigation of transition in a subsonic three-dimensional boundary layer. *Proc. DGLR Jahrestagung, Erlangen, Germany.*

BERTOLOTTI, F. P. & CROUCH, J. D. 1992 Simulation of boundary-layer transition: receptivity to spike stage. *Proc. 1st Euro. Comput. Fluid Dyn. Conf.* Elsevier.

BIPPES, H. 1972 Experimentelle Untersuchung des laminar-turbulenten Umschlags an einer parallel angeströmten konkaven Wand. *Heidelb. Akad. Wiss., Math. Naturwiss. Kl., Sitzungsber.* 3, 103–180.

BIPPES, H. 1991 Experiments on Transition in Three-Dimensional Accelerated Boundary-Layer Flows. *Proc. R.A.S. Conf. on Boundary-Layer Transition and Control, Cambridge, UK.*

BIPPES, H., MÜLLER, B. & WAGNER, M. 1991 Measurements and stability calculations of the disturbance growth in an unstable three-dimensional boundary layer. *Phys. Fluids* A **3**, 2371–2377.

BIPPES, H. & NITSCHKE-KOWSKY, P. 1990 Experimental study of instability modes in a three-dimensional boundary layer. *AIAA J.* **28**, 1758–1763.

BÖTTCHER, J. & WEDEMEYER, E. 1989 The flow downstream of screens and its influence on the flow in the stagnation region of cylindrical bodies. *J. Fluid Mech.* **204**, 501–522.

CORKE, T. C. & MANGANO, R. A. 1989 Resonant growth of three-dimensional modes in transitioning boundary layers. *J. Fluid Mech.* **209**, 93–150.

DEYHLE, H. 1993 Einfluß der äußeren Strömungsbedingungen auf den Transitionsprozeß einer dreidimensionalen Grenzschicht. Dissertation zum Dr.-Ing. an der TH Hannover, Mai 1993; published in *VDI Fortschritt-Bericht Reihe* 7, no 226. VDI-Verlag Düsseldorf (Germany).

DEYHLE, H., HÖHLER, G. & BIPPES, H. 1993 Experimental investigation of instability wave propagation in a 3-D boundary-layer flow. *AIAA J.* **31**, 637–645.

FISCHER, T. M. & DALLMANN, U. 1991 Primary and secondary stability analysis of a three-dimensional boundary-layer flow. *Phys. Fluids* A **3**, 2378–2391.

FISCHER, T. M., HEIN, S. & DALLMANN, U. 1993 A theoretical approach for describing secondary instability features in three-dimensional boundary-layer flows. *AIAA Paper* 93-0080.

GAPONENKO, V. R., IVANOV, A. V. & KACHANOV, Y. S. 1994 Experimental study of crossflow instability of a swept wing boundary layer with respect to travelling waves. *IUTAM Symp. on Laminar-Turbulent Transition, Sendai (Japan), Sept. 5–9.*

GOLDSTEIN, M. E. & HULTGREN, L. S. 1989 Boundary-layer receptivity to long-wave free-stream disturbances. *Ann. Rev. Fluid Mech.* **21**, 137–166.

HALL, P. 1983 The linear development of Görtler vortices in boundary layers. *J. Fluid Mech.* **130**, 41–57.

KACHANOV, Y. S. & TARARYKIN, O. I. 1989 The experimental investigation of stability and receptivity of a swept-wing flow. In *Laminar-Turbulent Transition, IUTAM Symp., Toulouse, France, 1989* (ed. D. Arnal & R. Michel), pp. 499–509. Springer.

KING, R. A. 1992 Three-dimensional boundary-layer transition on a cone at Mach 3.5. *Exps. Fluids* **13**, 305–314.

KOCH, W. 1992 On a degeneracy of temporal secondary instability modes in Blasius boundary-layer flow. *J. Fluid Mech.* **243**, 319–351.

KOHAMA, Y., SARIC, W. S. & HOOS, J. A. 1991 A high-frequency, secondary instability of crossflow vortices that leads to transition. *Proc. R.A.S. Conf. on Boundary-Layer Transition and Control, Cambridge, UK*, pp. 4.1–4.13.

KOSORYGIN, V. S., LEVCHENKO, V. Y. & POLYAKOV, N. P. 1984 On generation and evolution of waves in a laminar boundary layer. In *Laminar-Turbulent Transition, IUTAM Symp., Novosibirsk, USSR, 1984* (ed. V. V. Kozlov), pp. 233–242. Springer.

LEEHEY, P., GEDNEY, C. J. & HER, J. Y. 1984 The receptivity of a laminar boundary layer to external disturbances. In *Laminar-Turbulent Transition, IUTAM Symp., Novosibirsk, USSR, 1984* (ed. V. V. Kozlov), pp. 283–294. Springer.

LERCHE, T. & BIPPES, H. 1995 Experimental investigation of crossflow instability under the influence of controlled disturbance generation. *Colloq. Royal Netherlands Academy of Arts and Sciences on Transitional Boundary Layers in Aeronautics, Amsterdam (Netherlands), December 6–8 (Conf. Proc.).*

LIEPMANN, H. W., BROWN, G. L. & NOSENCHUCK, D. M. 1982 Control of laminar instability waves using a new technique. *J. Fluid Mech.* **118**, 187–200.

MALIK, M. R., LI, F. & CHANG, C.-L. 1994 Cross-flow disturbances in three-dimensional boundary layers: non-linear development, wave interaction and secondary instability. *J. Fluid Mech.* **268**, 1–36.

MEYER, F. 1989 Numerische Simulation der Transition in dreidimensionalen Grenzschichten. Dissertation zum Dr.Ing. an der Universität Fridericiana zu Karlsruhe (also DLR-FB 89–12).

MEYER, F. & KLEISER, L. 1989 Numerical simulation of transition due to cross-flow instability. In *Laminar-Turbulent Transition, IUTAM Symp., Toulouse, France, 1989* (ed. D. Arnal & R. Michel), pp. 609–619. Springer.

MORKOVIN, M. V. & RESHOTKO, E. 1989 Dialogue on progress and issues in stability and transition research. In *Laminar-Turbulent Transition, IUTAM Symp., Toulouse, France, 1989* (ed. D. Arnal & R. Michel), pp. 3–29. Springer.

MÜLLER, B. 1989 Experimental study of travelling waves in a three-dimensional boundary layer. In *Laminar-Turbulent Transition, IUTAM Symp., Toulouse, France, 1989* (ed. D. Arnal & R. Michel), pp. 489–498. Springer.

MÜLLER, B. 1990 Experimentelle Untersuchung der Querströmungsinstabilität im linearen und nichtlinearen Bereich des Transitionsgebietes. Dissertation zum Dr.-Ing. an der Universität Fridericiana zu Karlsruhe (also DLR-FB 90-09, 1990).

MÜLLER, B. & BIPPES, H. 1988 Experimental study of instability modes in a three-dimensional boundary layer. *Proc. AGARD Symp. on Fluid Dynamics of Three-Dimensional Turbulent Shear Flows and Transition, Cesme (Turkey), AGARD* CP-438, pp. 13-1–13-15.

MÜLLER, W. 1995 Numerische Untersuchung räumlicher Umschlagsvorgänge in dreidimensionalen Grenzschichtströmungen. Dissertation zum Dr.-Ing. an der Universität Stuttgart.

MÜLLER, W., BESTEK, H. & FASEL, H. 1994 Spatial direct simulation of transition in a three-dimensional boundary layer. In *IUTAM Symposium on Laminar-Turbulent Transition, Sendai (Japan), Sept. 5–9.*

NITSCHKE-KOWSKY, P. & BIPPES, H. 1988 Instability and transition of a three-dimensional boundary layer on a swept flat plate. *Phys. Fluids* **31**, 786–795.

PFENNINGER, W. & BACON, J. W. 1969 Amplified laminar boundary-layer oscillations and transition at the front attachment line of a 45° swept flat-nosed wing with and without boundary-layer suction. In *Viscous Drag Reduction* (ed. C. S. Well). Plenum.

POLL, D. I. A. 1985 Some observations of the transition process on the windward face of a long yawed cylinder. *J. Fluid Mech.* **150**, 329–356.

RADEZTSKY, R. H. JR, REIBERT, M. S. & SARIC, W. S. 1994 Development of stationary crossflow vortices on a swept wing. *AIAA Paper* 94-2373.

RADEZTSKY, R. H. JR, REIBERT, M. S., SARIC, W. S. & TAKAGI, S. 1993 Effect of micron-sized roughness on transition in swept-wing flows. *AIAA Paper* 93-0076.

REED, H. L. & SARIC, W. S. 1989 Stability of three-dimensional boundary layers. *Ann. Rev. Fluid Mech.* **21**, 235–284.

SARIC, W. S. 1992 Laminar-Turbulent Transition: Fundamentals. *AGARD Rep.* 786, *Special Course on Skin Friction Drag Reduction, VKI*, pp. 4-1–4-32.

SARIC, W. S. 1994 Low speed boundary-layer transition experiments. In *Transition: Experiments, Theory and Computations* (ed. T. C. Corke, G. Erlebacher & M. Y. Hussaini) Oxford University Press.

SCHUBAUER, G. B. & SKRAMSTAD, H. K. 1948 Laminary boundary-layer oscillations and transition on a flat plate. *NACA Rep.* 909.

SWEARINGEN, J. D. & BLACKWELDER, R. F. 1986 Spacing of streamwise vortices on concave walls. *AIAA J.* **24**, 1706–1709.

TAKAGI, S. & ITOH, N. 1994 Observation of travelling waves in a three-dimensional boundary layer along a yawed cylinder. *Fluid Dyn. Res.* **14**, 167–189.

TAKAGI, S., SARIC, W. S., RADEZTSKY, R. H., SPENCER, S. A. & ORR, D. J. 1991 Effect of sound and micron-sized roughness on crossflow dominated transition. *Bull. Am. Phys. Soc.*, **36**, 2630.

WAGNER, M. 1992 Numerische Untersuchungen zum laminar-turbulenten Übergang in zwei- und dreidimensionalen Grenzschichten. Dissertation zum Dr.Ing. an der Universität Fridericiana zu Karlsruhe (also DLR-FB 92-36).